TISSUE ENGINEERING: Part B
Volume 26, Number 1, 2020

DOI: 10.1089/ten.teb.2019.0296

termis
Tissue Engineering
& Regenerative Medicine
International Society

REVIEW ARTICLE

Photoacoustic Imaging in Tissue Engineering and Regenerative Medicine

Binita Shrestha, PhD,[1] Frank DeLuna, BS,[1] Mark A. Anastasio, PhD,[2] Jing Yong Ye, PhD,[1] and Eric M. Brey, PhD[1]

Several imaging modalities are available for investigation of the morphological, functional, and molecular features of engineered tissues in small animal models. While research in tissue engineering and regenerative medicine (TERM) would benefit from a comprehensive longitudinal analysis of new strategies, researchers have not always applied the most advanced methods. Photoacoustic imaging (PAI) is a rapidly emerging modality that has received significant attention due to its ability to exploit the strong endogenous contrast of optical methods with the high spatial resolution of ultrasound methods. Exogenous contrast agents can also be used in PAI for targeted imaging. Applications of PAI relevant to TERM include stem cell tracking, longitudinal monitoring of scaffolds *in vivo*, and evaluation of vascularization. In addition, the emerging capabilities of PAI applied to the detection and monitoring of cancer and other inflammatory diseases could be exploited by tissue engineers. This article provides an overview of the operating principles of PAI and its broad potential for application in TERM.

Keywords: photoacoustic imaging, tissue engineering, label-free vascular imaging, cell tracking and monitoring, scaffold imaging, assessment

Impact Statement

Photoacoustic imaging, a new hybrid imaging technique, has demonstrated high potential in the clinical diagnostic applications. The optical and acoustic aspect of the photoacoustic imaging system works in harmony to provide better resolution at greater tissue depth. Label-free imaging of vasculature with this imaging can be used to track and monitor disease, as well as the therapeutic progression of treatment. Photoacoustic imaging has been utilized in tissue engineering to some extent; however, the full benefit of this technique is yet to be explored. The increasing availability of commercial photoacoustic systems will make application as an imaging tool for tissue engineering application more feasible. This review first provides a brief description of photoacoustic imaging and summarizes its current and potential application in tissue engineering.

Introduction

The fields of tissue engineering and regenerative medicine (TERM) are primarily focused on the development of new sources of tissue or organs for replacement, regeneration, or reconstruction.[1] New approaches for the design of engineered tissues are continually under development and investigation.[2] However, tissue regeneration is a complex process modulated by multiple cues in the physiological environment. The better understanding of the interactions between engineered and host tissues is required for the design of new systems, but the tools available for evaluating this process are limited even in preclinical models. There is a significant need for new tools that enable monitoring and assessment of engineered tissues *in vivo* in animal models to enable the design and evaluation of next-generation tissue engineering strategies.[3]

Histological analysis is the gold standard for tissue evaluation. While histology provides crucial information, it is limited particularly when faced with unique aspects of tissue engineering. Histological analysis is generally an end point experiment precluding longitudinal monitoring or assessment. Besides, the processing required for histology can alter biomaterial structure in unpredictable ways, and the limited volume assessment can provide misleading results. A broad range of biomedical imaging technologies are available that may allow long-term monitoring of the morphological, functional, and molecular properties of

[1]Department of Biomedical Engineering, University of Texas at San Antonio, San Antonio, Texas.
[2]Department of Bioengineering, University of Illinois at Urbana-Champaign, Urbana, Illinois.

Table 1. Summary of Imaging Modalities in Tissue Engineering and Regenerative Medicine

Modality	*Resolution (μm)*	*Imaging depth (mm)*	*Application*	*Advantages*	*Limitations*
MRI	25–100	Full body	Tissue segregation and volume quantification[198,199] Monitoring cells and biomaterials[200–205] Cartilage imaging/ chondrogenesis,[206] osteogenesis,[207] angiogenesis[208] Vasculature characterization[209] Total blood volume and oxygenation[210–212]	No radiation Safe contrast agents No intra-arterial puncture Excellent soft tissue contrast Superior image quality	Spatial resolution is the inverse function of field of view Longer scan times Requires separate facility Strong magnetic field, limited real time imaging
X-ray/CT/μCT	1–100	Full body	Bone structure and morphology[213] Quantify tissue regeneration[214,215] Blood flow and perfusion[216] Neovascularization[217,218] Scaffold characterization[219,220] *In vivo* monitoring of biomaterials[221] Cell tracking and monitoring[222,223]	Nondestructive characterization of samples Superior resolution for microvasculature imaging Excellent image quality	Uses ionizing radiation energy Low soft tissue and biomaterial contrast Contrast agents may be toxic Long data acquisition Requires separate facility
PET/SPECT	1000	Full body	Cell tracking and monitoring[224–226] Perfusion[227,228] Angiogenesis[229] Molecular imaging[230]	Functional information High detection sensitivity Wide range of radiolabels available for molecular imaging	Uses ionizing radiation Do not provide structural information Poor spatial resolution Longer scan times Low signal to noise ratio Nonspecific uptake of radiotracers
US	30	300	Blood flow[231–233] Vascularization[234,235] Microvasculature imaging[54,236] Tissue regeneration[237–240] Tissue properties[241–243] Monitoring biomaterials or tissue engineered constructs[244–246]	Safe Portable Superior temporal resolution Higher imaging depth, Structural, mechanical (elastrography), and functional (Doppler) information	Anisotropic Limited soft tissue contrast Tradeoff between spatial resolution and imaging depth
MFM	1–1.6	0.5–1.0	Cell morphology and physiology[247–250] Cell distribution in scaffold[248] Biomaterial characterization[251–253] Cell tracking[254] Microvasculature morphology and oxygenation[250,255]	Superior spatial resolution Reduced photobleaching No photodamage	Limited imaging depth Limited *in vivo* application
OCT	1–15	2–3	Cell morphology and cell dynamics[256,257] Tissue development[258,259] Vascular imaging and perfusion[260–263] Biomaterial characterization[264–266] Blood flow[267,268]	Real time imaging High spatial and temporal resolution Does not require exogenous contrast agent Flow velocity independent of vessel orientation	Limited imaging depth, limited *in vivo* application

(*continued*)

TABLE 1. (CONTINUED)

Modality	*Resolution (μm)*	*Imaging depth (mm)*	*Application*	*Advantages*	*Limitations*
PAI	0.1–800	0.1–80	Total hemoglobin[269] Oxygen saturation[270,271] Metabolic rate of oxygen[50] Perfusion[272] Vasculature and angiogenesis[118,123,273] Blood flow[274] Cell tracking and monitoring[149,155,153] Biomaterial characterization[275,276]	Safe Real time imaging High imaging depth with reasonable spatial resolution Label free imaging of blood vessels Functional information Low background	No structural information Requires exogenous contrast agents for cellular imaging

CT, computed tomography; MFM, multi-photon fluorescence microscopy; MRI, magnetic resonance imaging; OCT, optical coherence tomography; PAI, photoacoustic imaging; PET/SPECT, positron emission tomography/single photon emission computed tomography; US, ultrasound.

engineered tissues. In addition, noninvasive imaging modalities may ultimately allow monitoring of therapeutic progress clinically as a potential guide for intervention if necessary.

The ideal characteristics of an imaging system depend, in part, on the application under evaluation. Desired characteristics for any imaging technique include (1) safe, (2) noninvasive, (3) high spatial resolution, (4) high tissue penetration, (5) quantitative, (6) functional, (7) allow longitudinal monitoring, (8) enable cell tracking, (9) provide information of biomaterial properties, and (10) free of exogenous labeling agents. Common imaging modalities such as magnetic resonance imaging (MRI), computed tomography (CT), and ultrasound (US) can achieve some of the characteristics.

Regardless of modality used, there is a natural give and take based on relative advantages and limitations in TERM applications (Table 1). For instance, MRI may have high spatial resolution and high tissue penetration, but it requires long scan times, is expensive, and may not enable material contrast. X-ray based imaging modalities (e.g., X-ray CT) provide superior resolution and imaging depth, but uses ionization radiation and provides limited soft-tissue contrast when used at a standard X-ray dose. US, in contrast, is safe and provides higher imaging depth, but generally has low spatial resolution for the TERM application. Therefore, the continued development and application of new imaging tools would benefit the TERM fields.

Photoacoustic imaging (PAI) system has emerged as a promising alternative for biomedical imaging for TERM applications.[4–9] PAI has been extensively investigated in biomedical imaging such as cancer diagnosis, cardiovascular diseases, and neurology to name a few. While the PA effect was first discovered by Alexander Bell in the 18th century,[10] its rapid progress in the past few decades is fueled by fast-paced advancement in laser technology and emerging fundamental research in PAI. PAI, also known as optoacoustic imaging, is a hybrid technique meaning it exploits two different phenomena, optical and acoustic, to generate images. When an optical pulse from a laser is used to excite a tissue, optical absorption results in a transient local thermal expansion of tissues. Thermal expansion leads to a change in pressure distribution in the tissues and the generation of broadband ultrasonic waves. The resultant acoustic signals can then be detected outside the tissue for reconstruction.[5,6] The reconstructed image depicts a map of initial pressure distribution that is proportional to absorbed optical energy.[11] These images provide anatomical, functional, and molecular information of biological tissues.

PAI generally offers a high spatial resolution, increased imaging depth relative to most optical methods, label-free vascular imaging, and retrieval of functional and molecular information. In addition, extrinsic contrast agents can be used to generate or enhance PA contrast. Moreover, PAI does not use ionizing radiation, and therefore, PAI demonstrates high potential for clinical applications where safety is an important concern. As there are a number of excellent review articles on PAI,[4,5,6–9,11] we provide only a brief overview of three major modalities of PAI: PA computed tomography (PACT), PA microscopy (PAM), and multispectral PAI. The bulk of the review focuses on current and potential applications of PAI in TERM.

Basic Image Formation Principles of PAI

Optical imaging plays an important role in preclinical and clinical studies. However, it suffers from poor spatial resolution at depth due to light diffusion in highly scattering tissues.[12] Conventional optical imaging techniques, including confocal microscopy and two-photon fluorescence microscopy, have an imaging depth typically limited to <1 mm.[13] In contrast, US images can be obtained at a much deeper tissue level (a few centimeters). However, US imaging does not provide molecular specificity and its image quality typically has low contrast limited by the US contrast mechanism that depends on the mechanical and elastic properties of the tissue rather than individual molecules.[8,9] PAI has emerged as a promising modality to address many of the most challenging issues in conventional optical and US imaging methods. It is based on a hybrid technology that combines rich optical contrast mechanisms and superior ultrasonic penetration depth and resolution.[5–8,14–16] For PAI, photons from a nanosecond laser pulse are absorbed by certain endogenous chromophores or exogenous contrast agents in a tissue sample, causing impulsive heating and acoustic stress. The acoustic stress relaxes by launching broadband US pressure waves (i.e., PA emission), which propagate to the outside of the tissue and are detected by a mechanically scanned US receiver or an array of US receivers to form PA images.[5,17,18] For effective PA signal

generation, it is necessary to reach the so-called thermal and stress confinement conditions using a pulsed laser with its pulse duration normally within several nanoseconds, so that the thermal diffusion and stress relaxation can be neglected during the laser illumination period.[4] The initial pressure, P_0, generated by an optical absorber is determined by the expression $P_0 = \Gamma \mu_a F$, where μ_a is the optical absorption coefficient of the photoabsorber, F is the fluence of the light at the photoabsorber, and Γ is the tissue's Grüneisen parameter.[18,19] The Grüneisen parameter is related to the tissue properties and can be further expressed as $\Gamma = \beta c^2/C_p = \beta/(\kappa \rho C_p)$, where β is the isobaric volume expansion coefficient, C_p is the specific heat, c is the acoustic speed, κ is the isothermal compressibility, and ρ is the mass density.[5,19]

Since acoustic waves scatter much less than optical waves in tissue, PAI allows for deep-tissue imaging by leveraging the acoustic signals originated from optical absorption and offers advantages of rich endogenous and exogenous optical contrast agents for functional molecular imaging without the use of ionizing radiation.[20]

Photoacoustic Computed Tomography

In a canonical PACT experiment, an expanded laser beam is used to irradiate the whole tissue region of interest. PA waves generated from the whole volume of the targeted tissue are detected by an US detection system that completely or partially surrounds the object. From the detected acoustic signals, a reconstruction algorithm is utilized to form an image that depicts the distribution of the initial PA-induced pressure distribution P_0, or equivalently, if the Grüneisen parameter is known, the distribution of the absorbed optical energy. Depending on the imaging system design, the reconstructed image can be two dimensional (2D) or three dimensional (3D). For example, a recent report has demonstrated the development of a 2D PACT system for imaging detailed angiographic structures in human breasts within a single-breath hold.[21] PACT allows its spatial resolution to be scaled with the desired imaging depth in tissue at a high depth-to-resolution ratio. It can reach up to 7 cm into a tissue while maintaining a good spatial resolution on the order of 1/200 of the desired imaging depth.[8] In the past decade, extensive studies have demonstrated the applications of PACT for multiscale and multicontrast images, which reveal a tissue's anatomical, functional, metabolic, and histologic properties based on endogenous contrast, and provide molecular and cellular specificity based on exogenous contrast agents.[8,9,22]

Similar to other computed imaging modalities such as X-ray CT and MRI, image quality in PACT will be influenced by the quality of measurement data and the choice of image reconstruction algorithm used. An extensive effort from many research groups has been devoted to the development of different approaches for image reconstruction in PACT.[11] Multiple reported approaches, including filtered back-projection,[23,24] model-based inversion algorithms,[25–27] and wavelet-based approaches,[28,29] have been demonstrated to provide a successful mapping of the distributions of targeted optical absorbers in a 3D tissue volume. Most of the reported implementations of PACT sought to reconstruct estimates of the PA-induced pressure distribution. Active research for developing new image reconstruction algorithms is undergoing to correct the artifacts and distortions in PACT images due to tissue heterogeneity.[30–32] For example, researchers are currently developing a transcranial image reconstruction algorithm to compensate for the effects of wave propagation through the skull to better image the brain.[33,34] Quantitative PACT methods seek to obtain accurate estimates of the medium's optical parameters. Obtaining absolute chromophore concentrations from PA images obtained at multiple wavelengths is a nontrivial aspect of PAI but is essential for accurate functional and molecular imaging.[7] However, such methods are still in a stage of development and have not been widely validated.[35]

Photoacoustic microscopy

In contrast to PACT for deep tissue imaging, PAM is used to achieve superior high-resolution imaging, although its imaging depth is limited. PAM typically utilizes a confocal configuration by having overlapped foci of both the optical excitation and ultrasonic detection to optimize its sensitivity and resolution.[36] As the time-of-flight information of the PA signal provides the axial resolution, each focused laser beam position produces a depth-resolved one-dimension (line) image into the tissue without mechanical scanning. Thus, a 2D transverse scanning of the laser beam (together with the US receiver) generates a 3D image. The lateral resolution is determined by the product of the point spread functions of the laser focus and acoustic detection focus.[37] Optical-resolution PAM (OR-PAM) can be achieved when the optical focus is significantly tighter than the acoustic focus.[38] Even though other optical imaging techniques, such as confocal and two-photon fluorescence microscopy, also provide high-resolution imaging (spatial resolution of 1–2 μm) capability at an imaging depth similar to that of PAM (0.2–1 mm depth), PAM possesses a unique feature for label-free imaging with optical absorption as a contrast. For example, *in vivo* label-free functional imaging of hemoglobin oxygen saturation (sO2) in single blood capillaries can be imaged clearly with OR-PAM (Fig. 1).[38] Different from PACT, image formation for PAM is relatively straightforward and does not require the use of complicated image reconstruction algorithms, as it utilizes direct image formation principles.

Multispectral imaging

In this section, we will discuss the principle of multispectral PAI and its pertinent applications in tissue engineering. In addition, we will briefly cover the use of multispectral imaging for quantitative PACT.

PAI at a single optical excitation wavelength can spatially resolve certain photoabsorbers with a distinct absorption spectrum. However, for samples containing multiple absorbers with overlapped absorption spectra, the different sources of absorption cannot be distinguished from one another if PAI is conducted at a single excitation wavelength. This situation is not uncommon especially for *in vivo* studies, as the spectra of the targeted photoabsorber may overlap with other endogenous photoabsorbers or other exogenous contrast agents used to label different tissues.[39] In such a situation, multispectral PAI is required to identify the photoabsorbers of interest through their unique absorption spectra through spectral unmixing.

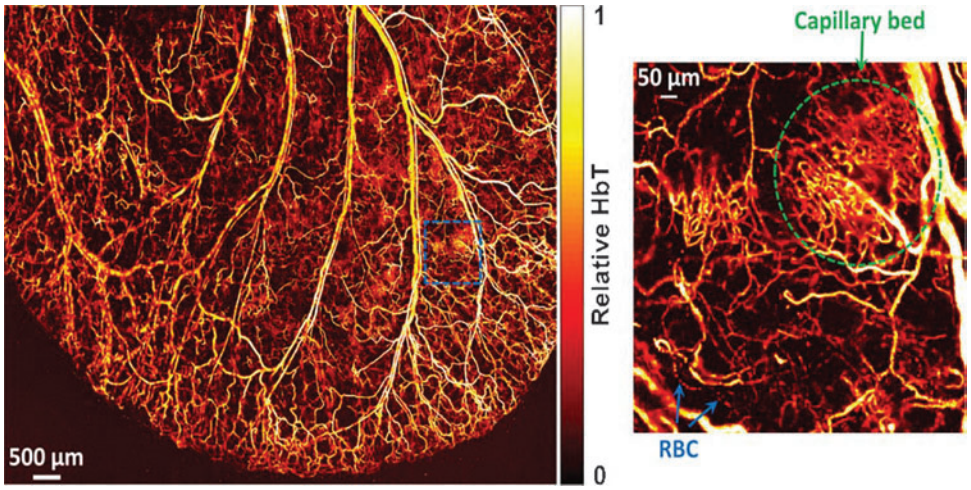

FIG. 1. OR-PAM of relative total hemoglobin concentration (HbT) in a living mouse ear, revealing the vascular anatomy. Insert shows a densely packed capillary bed and individual red blood cells traveling along a capillary. © 2011 Reprinted with permission of Optical Society of America.[38] OR-PAM, optical-resolution PAM. Color images are available online.

Spectral unmixing algorithms are applied to the resulting images obtained at multiple excitation wavelengths to distinguish targeted photoabsorbers (whether endogenous and/or exogenous) with overlapped absorption spectra.[40] In short, 2D spectral unmixing commonly adopts a linear mixture model, which assumes that the measured spectrum at each image location $M(r, \lambda)$ (function of position, r, and wavelength, λ) is a linear combination of the spectral signals, $S_i(\lambda)$, of k distinct materials, weighted by their relative concentration(s) at that specific location, $c_i(r)$: $M(r,\lambda) = \sum_{i=1}^{k} S_i(\lambda)c_i(r)$.[40,41] With spectral unmixing, the spatial distribution of multiple photoabsorbers with overlapped absorption spectra can all be mapped separately. However, the unmixing of 3D images is complicated by light fluence attenuation as a function of tissue depth and the wavelength used, which is fundamentally a nonlinear inversion problem. The unknown depth-dependent and wavelength-dependent fluence, $\Phi(r, \lambda)$, introduces changes to the detected PA spectra, $P(r, \lambda)$, corresponding to depth, termed "spectral coloring": $P(r,\lambda) \sim \Phi(r,\lambda)$.[7,41] Therefore, the detected spectrum in 3D PAI will vary according to its location in the tissue and influenced by the combination of the tissue-specific optical properties along the optical path being irradiated.

Quantitative PAI is a technique that aims at obtaining/estimating the absolute concentrations of the present chromophores from PA images.[7] As the attenuation of light, even at a fixed depth, can vary with the excitation wavelength used, it is challenging to accurately quantify the concentration of the targeted photoabsorber. Therefore, it is of great interest to develop novel methods to correct/overcome this challenge to obtain quantitative results in deep tissue. There are multiple ongoing studies on this topic as reported recently.[7,42,43] The most common method hinges on multispectral imaging to estimate the optical absorption and scattering coefficients. Once determined, estimates of local concentrations of absorbers can be calculated, with the most common one being hemoglobin oxygen saturation (sO_2).

To summarize, by leveraging the use of multiple excitation wavelengths in conjugation with either PACT or PAM, multispectral imaging can offer an analysis of multiple endogenous and exogenous contrast agents concurrently in real time. Currently, these multispectral imaging techniques have been used to image blood vessels,[44] quantify oxygen saturation levels,[45] identify/monitor melanoma,[46] detect lipids in vessels,[47] and to detect and characterize glioblastoma,[48] to name a few of the multitude of applications capable with this powerful technique.

Contrast in PAI

Several contrast mechanisms can be exploited in PAI to provide insight into engineered tissues. Contrast agents can be categorized as endogenous and exogenous agents. One of the exciting aspects of PAI is the differential optical absorption of endogenous chromophores that provides intrinsic contrast. Intrinsic optical absorbers such as blood, lipid, melanin, and collagen can be imaged with PAI without the need for additional contrast agents (Fig. 2). Multispectral analysis can allow identification and separation of distinct optical absorbers. In addition, exogenous contrast agents can be introduced to enhance detection sensitivity and to target specific structures, molecules, or cells.

Endogenous contrast agent

Common endogenous contrast agents, including blood, lipid, and melanin, have been widely investigated to predict, detect, or monitor a variety of disease conditions ranging from cancer to inflammatory diseases, such as atherosclerosis. The sections below provide examples of how endogenous contrast has been exploited to provide insight into tissue features relevant to TERM applications.

Blood. Blood is the most studied endogenous contrast agent for PAI. The absorbance of blood is in a broad spectral range and is significantly higher relative to other common chromophores, at least by an order of magnitude. As a result, functional vasculature (i.e., vasculature containing blood) generates significant contrast with PAI. This contrast can be used to quantify the microvascular density and evaluate vascular network structure. The optical absorption of blood is primarily due to hemoglobin. The absorption properties of hemoglobin are dependent on its oxygenated (HbO2) or deoxygenated (Hb) state. This optical property of blood allows PAI to determine total hemoglobin concentration, oxygen saturation level of blood, differentiate between veins from arteries, and blood flow speed (Fig. 3).[49]

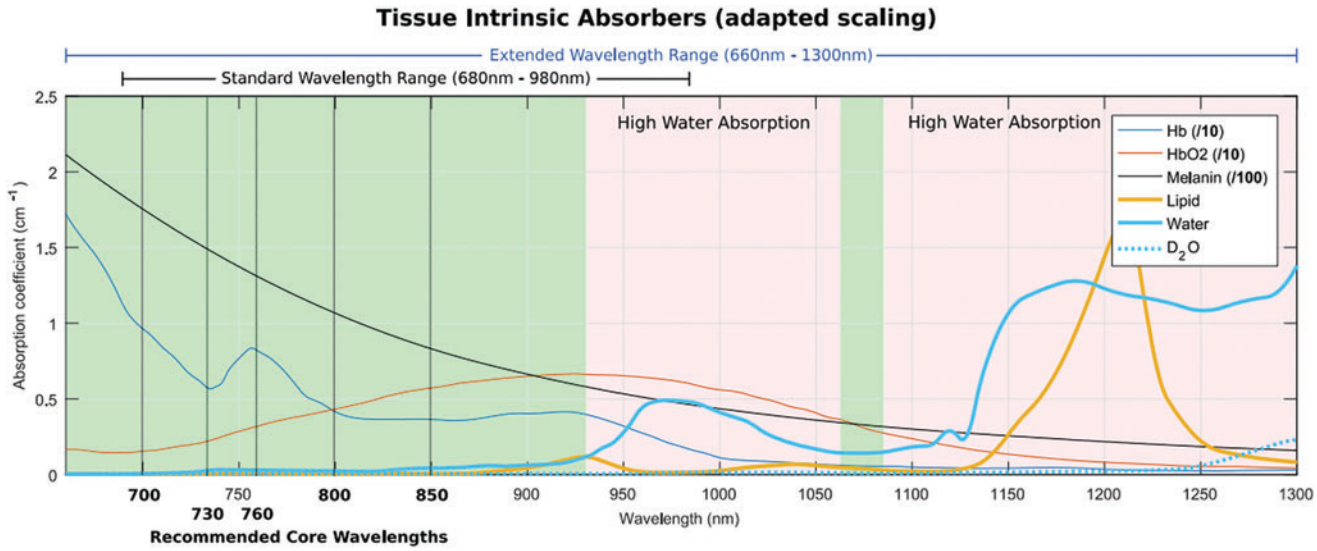

FIG. 2. Absorbance spectra of endogenous contrast agents. © 2012 Reprinted with permission from iThera Medical, Inc. Color images are available online.

These features result in extensive applications of PAI in diagnosis, monitoring, or evaluation of conditions that are typically characterized by alterations in vasculature such as cancer and cardiovascular diseases.[50] Vascularization is also critical for the clinical success of engineered tissues, making this an important feature of PAI.[51] In PA, signal generation is independent of the movement of the absorber (i.e., hemoglobin). Other commonly used tools, such as power doppler imaging, require movement of blood and which can result in false positive or undetected vessels.[52,53]

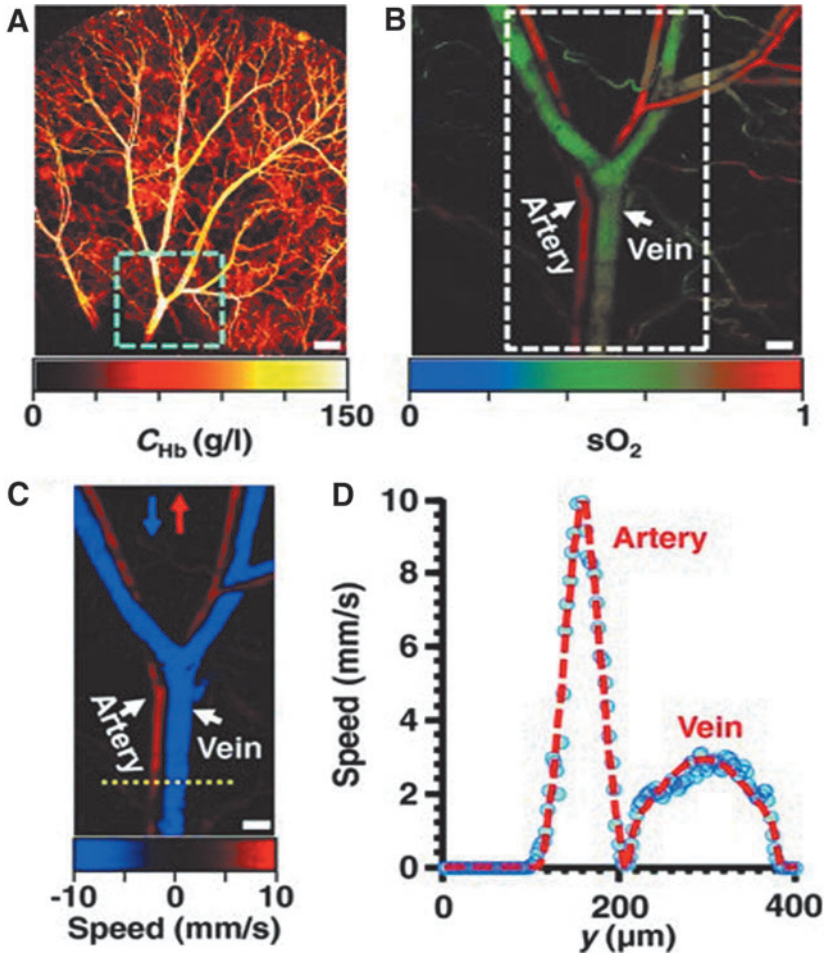

FIG. 3. Metabolic PAM images. **(A)** Metabolic PAM image of total concentration of hemoglobin (CHb) **(B)** metabolic image of hemoglobin oxygen saturation (sO_2) of area inside the dashed box **(C)** *Red arrow* indicates positive scanning direction, and *blue arrow* indicates negative scanning direction and **(D)** Speed of blood flow across the *dashed line* in **(C)**. Scale bar: **(A)** 500 μm **(B, C)** 125 μm. © 2011 Reprinted with permission from Society of Photo-Optical Instrumentation Engineers (SPIE).[49] Color images are available online.

Lipid/fat. Lipids exhibit absorbance in the range between 1150 and 1310 nm.[54] The strong absorption of lipids has enabled intravascular lipid deposition to be detected with PAI.[55] Lipid deposition inside the arterial wall is increased in atherosclerosis, a harbinger of many cardiovascular diseases. In addition to diagnosis, PAI of lipids can also be used to characterize the lipid content and its spatial distribution within plaques and thus can be used to monitor disease progression.[56] Wang *et al.* reported the presence of a ''valley'' in the water absorption spectra between 1450 and 1900 nm. Based on this result, they reported a new optical window for deep tissue imaging from 1600 to 1850 nm, where the absorption of pure water is comparable to the absorption coefficient of heme protein at 800 nm.[57] Spectral features of C-H overtones within this range demonstrated label-free detection of arterial plaques. Lipids are rich in CH_2 groups, and therefore, CH_2 overtones can distinguish the presence of lipids at 1.7 μm wavelength through the layer of blood.[58–60]

Melanin. Melanin is a group of natural pigments that determine skin color. Melanocytes are the cells that play a crucial role in the production and distribution of melanin. Melanin exhibits a strong absorbance (1000 times than water) in the visible range of 700–730 nm. At these wavelengths, melanin demonstrates high contrast relative to other endogenous contrast agents. Melanin PAI has mostly been investigated to diagnose or monitor the progression of Melanoma, a skin cancer that arises from mutation of melanocytes.[61,62]

Collagen. Collagen is the most abundant protein in the body and a key component of the extracellular matrix in many tissues and organs. Collagen imaging may allow disease diagnosis and monitoring of disease progression.[63,64] For example, Kruizinga *et al.* showed that lipid and collagen could be differentiated in the arterial wall for the detection of atherosclerotic lesions.[65] However, the absolute spectrum of collagen is not well established, partly due to the high scattering and fluorescence properties of collagen in the visible range. In addition, a tunable laser system that operates in the range of above 1000 nm is required to evaluate the absorbance of collagen.[66] Recently, Sekar *et al.* compared collagen absorption in the visible and short wave infrared region (SWIR). They reported higher absorption of collagen in the range of 1.1–1.7 μm than in the visible range of the spectrum. On further comparison within the SWIR range, they observed collagen absorption to be 5 times higher than lipids at 1700 nm and 1.5 times higher at 1100 nm.[67] Similar to lipids, Wang *et al.* have reported that vibrational overtone absorption of CH_3 group can distinguish collagen in PAI.[60]

Exogenous contrast agent

PAI without the introduction of exogenous contrast has been widely studied and shown to be useful in a variety of applications. Nevertheless, there are many limitations with relying solely on label-free imaging. Contrast agents have played an important role in molecular imaging, due to their versatility, customizability (for specific applications) and ease of use. There are various principles, materials, shapes, and sizes of contrast agents suitable for different imaging modalities. Ideal contrast agents could significantly increase contrasts, effectively improve imaging depth or accuracy, and provide pertinent molecular specific information.[68–70] In this section, a short review about various exogenous contrast agents for PA molecular imaging is presented.

Synthetic near infrared dyes. There are many biocompatible dyes that absorb in the near infrared (NIR) optical window,[71] including heptamethine cyanine dyes (i.e., Indocyanine Green [ICG], and the IRDye family [range from 680 to 800 nm]), borondipyrromethene dyes (i.e., the AlexaFluoro family [range from 650 to 790 nm]), squaraine dyes (i.e., D1[72,73]), rhodamine dyes, and azo dyes (i.e., methylene blue), which have all been used extensively in PAI. These dyes are typically small molecules, on the order of 1 nm, and are able to quickly clear the body through the renal system. Many of these dyes are fluorescent and are commonly used in purely optical imaging. For PAI, the PA emission comes from the energy due to the optical absorption. A low fluorescence quantum yield of the dye results in more efficient PA signal generation, as more of the absorbed energy is converted into the PA signal rather than being emitted as fluorescence.[68]

It has been shown that to obtain static contrast in PAI, a NIR dye such as ICG can be detected at nanomolar concentrations in tissue.[8,74] However, with respect to responsive imaging probes for PAI, very few reports are currently available. One such report by Mishra *et al.*, demonstrated the development of a metallochromic sensor utilizing a heptamethine cyanine dye, IR780, to measure calcium concentrations.[75] Quantifying calcium ion concentrations pertain to many biological processes/responses. Specifically, pertaining to bone tissue regeneration, calcium is a fundamental building block of the native extracellular matrix,[76] as well as being shown to have a significant role in osteogenic differentiation,[77] making it an ideal candidate for molecular PAI in tissue engineering.

NIR protein dyes. With the steady rise in applications capable with PAI, synthetic dyes (which require methods for target and delivery) present many hindrances for more longitudinally relevant applications. Protein dyes, as conventionally used in optical imaging, can be genetically encoded, thus ever present in a targeted sample *in vivo*, allowing for a multitude of imaging applications. One particular family of the dyes that shows great promise for PAI is the iRFP family.[78–81] With optical absorptions in the range of 650–750 nm and a low quantum yield (for better PA signal generation), they can be coupled with gene-delivery technologies (i.e., CRISPR) to be a powerful tool for the targeting, labeling, and longitudinal monitoring of specific cell groups *in vivo*.[82]

Plasmon nanoparticles. Noble metal (i.e., gold and silver) nanoparticles (NPs) have been widely used as PA contrast agents. This is primarily due to their strong and tunable optical absorption that results from the surface plasmon resonance (SPR) effect. The SPR effect occurs when free charges on the surface of noble metal NPs oscillate in concert with the electromagnetic field, resulting in an optical absorption that is five orders of magnitude greater

than dyes (on a per-particle basis). When the size and shape of the NP change, so does its resonant frequency. For example, as a gold nanorod grows longer, its peak absorption shifts to longer wavelengths.[83] The ideal wavelength for absorption depends on the other endogenous and exogenous absorbers in the region and the excitation wavelengths available for imaging. In addition to being highly tunable, gold NPs (GNPs) form strong gold-thiolate bonds that enable covalent surface modification, such as polyethylene glycol functionalization, for increasing biocompatibility[84] and active targeting (i.e., antibody conjugations).[68] Furthermore, utilizing a silica coating around GNPs can both increase PA stability,[85] allowing for longer image times without damaging the contrast agent, while also increasing the PA signal generation,[86] for better image quality.

The field of stem cell therapy is currently advancing toward clinical trials in a variety of biomedical applications, most notably in the field of TERM.[87–91] This advancement leads to the new requirements of medical imaging to monitor stem cell therapies (i.e., stem cell tracking). One example of utilizing plasmonic NPs to meet the demands of monitoring novel stem cell therapies was reported by Ricles *et al.* They showed the use of a dual GNP system in conjunction with PACT for the monitoring of both implanted mesenchymal stem cells, loaded with gold nanorods, and infiltrating macrophages, loaded with gold nanospheres, to the wounded area.[92]

Carbon nanostructures. Carbon forms different allotropic structures as follows: carbon nanotubes, graphene-based nanomaterials, and nanodiamonds. All three classes can be synthesized to possess an intrinsic absorption in the NIR range and thus play an important role for PAI. Despite possessing a lower molar extinction coefficient than gold, carbon NPs (CNPs) hold significant potential for molecular PAI due to their flexibility of synthesis and functionalization.[93,94] CNPs can be also conjugated with plasmonic NPs to further enhance their PA emission properties. For example, fluorescent nanodiamonds (FNDs), a novel nanomaterial that has been utilized for biomedical imaging applications due to its excellent photostability, high biocompatibility, and extended far-red fluorescence emission,[95] may also be utilized as a PA contrast agent by conjugating them with GNPs.[96] It has been demonstrated that their PA signals can be significantly enhanced by a factor of 30 when the FNDs are conjugated with GNPs. The large increase in the PA signal has been attributed to the local field enhancement of the GNPs and the energy transfer between FNDs and GNPs, which increases the nonradiative decay processes of FNDs through fluorescence quenching, thus enhancing the conversion efficiency of the absorbed laser energy into heat for enhanced thermoelastic effects (i.e., PA signal generation).[96]

One example of utilizing carbon nanostructures in tissue engineering was reported by Cai *et al.*, where single-walled carbon-nanotubes (SWNTs) were incorporated in poly(lactic-co-glycolic acid) (PLGA) polymer scaffolds to both image and characterize the scaffold through PAM.[97] Characterization and longitudinal monitoring of porous polymeric scaffolds are critical, as these structures are vital in the development of neo-tissue formation, as they provide structural support, and can be integrated to house implanted cells and elude pertinent growth factors.[98]

Polymer NPs. There are many different polymer NPs, in which their strength comes from their ease of customizability (i.e., conjugations with other NPs or dyes, encapsulations of other NPs or dyes, and functionalization for molecular targeting). Organic semiconducting polymer NPs prepared from semiconducting polymers are promising nanoagents with excellent optical properties for imaging and therapy and have been demonstrated in PAI.[99] Conjugated polymers are macromolecular structures with a highly delocalized conjugated backbone. The conjugated system is spread through the entire polymer backbone, and the polymers are densely packed into NPs, yielding much higher extinction coefficients and photostability than possible with small molecule dyes. One can tune the optical properties (which are strongly dependent on the conjugated core) by adopting different backbone structures, combining different conjugated polymers, and controlling aggregation and surface functionalization.[100]

Wound healing and regenerative medicine go hand in hand. Whether implanting an engineered biomaterial or transplanting stem cells, the wound healing process follows the required invasive procedure.[101] pH is a recognized indicator of the state of the wound, providing information about bacterial contamination and the stage of healing.[102] Pu *et al.* have reported a novel PA pH-dependent contrast agent, made of semiconducting polymer NPs in response to reactive oxygen species.[103] This can potentially be implemented to work in conjugation with PACT to monitor pH *in vivo*, thus wound healing, following biomaterial or stem cell therapies.

Table 2 summarizes the different types of exogenous contrast agents used in PAI, its application in tissue engineering, and general limitations.

PAI in TERM

Tissue engineering scaffolds

Biomaterial scaffolds, both natural and synthetic, are often a fundamental component of a successful tissue engineering strategy. The scaffolds provide physical support for tissue growth but also can directly modulate cell activity and function.[104] The physical, chemical, and mechanical properties of tissue engineering scaffolds play a vital role in cell migration, proliferation, and differentiation,[105] and changes in these properties due to degradation (intentional or not) can facilitate the success or failure of the tissue. Substantial scaffold degradation studies are often performed *in vitro* before implantation, but the characterization of degradation *in vivo* is a significant challenge in tissue engineering.[3] Longitudinal quantitative analysis of the scaffolds can provide information that is critical to understanding the behavior of the materials *in vivo*. In addition, tools that allow evaluation of cell-scaffold interactions *in vivo* may provide important cues in understanding cell behavior in tissue engineering systems.

Common imaging modalities, including CT and scanning electron microscope (SEM), are used for preimplantation characterization of scaffold structure. However, SEM cannot be applied to image implanted samples and most

Table 2. Summary of Exogenous Photoacoustic Contrast Agents Used in Tissue Engineering and Regenerative Medicine

Contrast classification	*Type*	*Name*	*Spectral absorption, λ (NM)*	*Applications pertinent to TERM*	*General limitation*
Synthetic NIR dyes	Heptamethine cyanin dyes	Indocyanine green	780	Synthetic dyes are easily customizable and are commercially available with a multitude of functional groups (i.e., amine, biotin, N-(hydroxysuccinimide)) already attached for simple conjugation to other NPs or targeting ligands for functional imaging. TERM relies greatly on being able to distinguish between tissues (i.e., cells before and after differentiation), thus utilizing a targeting ligand and a high PA generating dye is a simple, yet effective method for imaging.	While Synthetic dyes are simple and easy to use (as it's the same as doing conventional optical imaging), it falters in a few key aspects; (1) compared to NPs (gold or polymer) synthetic dyes generally generate less PA signal, (2) they clear the renal system quite quickly, meaning that without targeting, imaging time is cut short (and is nonfunctional), and (3) these dyes photo-bleach and are not ever-present in the tissue, like a report gene would be, meaning longitudinal studies would be rather difficult if not impossible.
		IRDye800CW	778		
		IRDye800RS	770		
		IRDye800	795		
		IRDye750	766		
		IRDye700DX	680		
		IRDye700	685		
		IRDye680RD	680		
		IRDye680LT	680		
		IRDye650	651		
		CDnir7	806		
		IC-5-T	830		
		IC7-1-Bu	823		
	Borondipyrronmethene dyes	Alexa Fluor 790	782		
		Alexa Fluor 750	749		
		Alexa Fluor 700	702		
		Alexa Fluor 680	679		
		Alexa Fluor 660	663		
	Squaraine dyes	D1	867		
	Rhodamine dyes	Rhodamine B	610		
	Azo dyes	Methylene blue	664		
		Evans blue	620		
NIR protein dyes	iRFP	iRFP720	702	A protein dyes' greatest strength is in its ability to be genetically encodable, allowing for the dye to be ever present, and even engineered to be functional such as calcium sensitive GFP (GCamP). Leveraging this aspect can allow for TERM researchers to tag or monitor specific cell groups over long periods of time.	The field of utilizing NIR protein dyes for PAI is still in its infancy. Meaning utilization of these techniques need to first be established before TERM research.
		iRFP713	690		
		iRFP702	673		
		iRFP682	663		
		iRFP670	643		
		PAiRFP1	659		
		PAiRFP2	692		

(*continued*)

Table 2. (Continued)

Contrast classification	*Type*	*Name*	*Spectral absorption, λ (NM)*	*Applications pertinent to TERM*	*General limitation*
Plasmonic NPs	Gold NPs	Gold nanospheres	Tunable	Gold NPs are generally attributed in having the highest PA signal generation. They are both easily synthesized and functionalized (to control spectral absorption and increase biocompatibility). NPs can easily be incorporated into biomaterials for long-term imaging *in vivo*.	Generally, TERM and nanoscience are not always intertwined. NPs may have adverse effects to the studies conducted in TERM research. Meaning, both caution and preliminary studies exploring cytotoxicity, as well as other relevant biological effects (i.e., uptake, changes to cell morphology, inhibiting biochemical stimulus, and so on) should be conducted before utilizing them in a study.
		Gold nanorods	Tunable		
		Gold nanostars	Tunable		
		Gold nanocubes	Tunable		
		Gold nanoshells	Tunable		
	Silver NPs	Silver nanospheres	Tunable		
Carbon nanostructures	Graphene oxide	GO nano-particles	Tunable	Similar to plasmonic NPs, carbon nanostructures are both easily synthesized and functionalized (to control spectral absorption and increase biocompatibility). They can be incorporated into biomaterials or conjugated to other contrast agents for increased PA signal generation.	Carbon Nanostructures are generally limited by their broad absorption profiles and low molar extinction coefficient, thus a lower PA signal generation. Similar to Plasmonic NPs, carbon nanostructures may have adverse effects to the studies conducted in TERM research.
		rGO nano-particles	Tunable		
	Carbon nanotubes	SWNTs	Tunable		
		MWNTs	Tunable		
	Nanodiamonds	Nano-diamonds	Tunable		
		Fluorescent nano-diamonds	Tunable		
Polymer NPs	OSPNs		Tunable	Polymer NPs are attractive contrast agents for their great biocompatibility, as well as their broad range of functionalization. Furthermore, they can be utilized as encapsulating NPs, so not only are they useful for imaging but also can be utilized as a method for biochemical stimulus (i.e., growth factors, or drugs).	Polymer NPs are extremely broad and intrinsically different to one another. Generally, they're limited by their novelty, as little knowledge is known on how their PA signal generation may change due to the NP's structure and influence from other local signaling compounds (endogenous or exogenous).
	Conjugated polymers		Tunable		

MWNTs, multi-walled carbon nanotubes; NIR, near infrared; NPs, nanoparticles; OSPNs, organic semiconducting polymer NPs; PA, photoacoustic; PAI, photoacoustic imaging; SWNT, single-walled carbon-nanotube; TERM, tissue engineering and regenerative medicine.

biomaterials do not generate sufficient contrast for imaging with CT under *in vivo* conditions. Besides, imaging of cells within scaffolds is often performed by staining with osmium tetroxide, which requires harvest and postprocessing.[106,107] PAI has been explored as an alternative technique for imaging polymeric scaffolds and the cells cultured in these scaffolds. Usually polymer itself does not generate enough PA signal for PA contrast; therefore, contrast agents are incorporated into biomaterial scaffolds to enhance PA contrast. In the absence of intrinsic cellular contrast, exogenous contrast agents such as dyes or NPs can be incorporated into cells[108–110] or biomaterial scaffolds to enhance PA contrast.[111] For instance, SWNTs were entrapped in PLGA scaffolds for mechanical reinforcement and to provide PAI contrast.[97] Both OR-PAM and acoustic resolution PAM (AR-PAM) were used to characterize average porosity and pore size of PLGA scaffolds immersed in a biological buffer. Micro CT images of dry and wet scaffolds were taken for the comparisons. Micro-CT images of dry samples clearly depicted well resolved porous structure. However, wet scaffolds (immersed in fetal bovine serum) failed to provide any structural details. The structural details from PAM images agreed well with measurements obtained by micro CT of dry scaffolds. To evaluate scaffolds in an environment mimicking *in vivo* imaging, the scaffolds were embedded in chicken breast tissue. With ~660 μm tissue penetration depth and lateral resolution of 2.6 μm, OR-PAM images depicted detailed structures of the scaffold that was comparable to that of an optical microscope such as one-photon fluorescence microscope. AR-PAM, in contrast, was able to image scaffold through 1.7 mm of soft chicken tissue. The lateral resolution of AR-PAM is less (45 μm), but able to achieve greater tissue depth. As resolution depends on the penetration of US signals, the deeper tissue penetration typically corresponds with a sacrifice in lateral resolution.

PA has received significant attention largely due to its advantages for noninvasive imaging in people or animal models.[112] Talukdar *et al.* used PA and US imaging concomitantly to image SWNT-PLGA scaffolds *ex vivo*, as well as *in vivo*.[113] In this study, US images provided the anatomical location of the scaffold, whereas PA images provided the blood oxygen saturation maps around and within the scaffolds which is difficult to achieve with other imaging modalities. PLGA and PLGA-SWNT scaffolds were first embedded in the chicken breast tissue of varying thickness for *ex-vivo* testing (Fig. 4). For *in vivo* imaging, the scaffolds were implanted subcutaneously in rats at ~2 mm depth. The PA and spectroscopic images (blood oxygen saturation

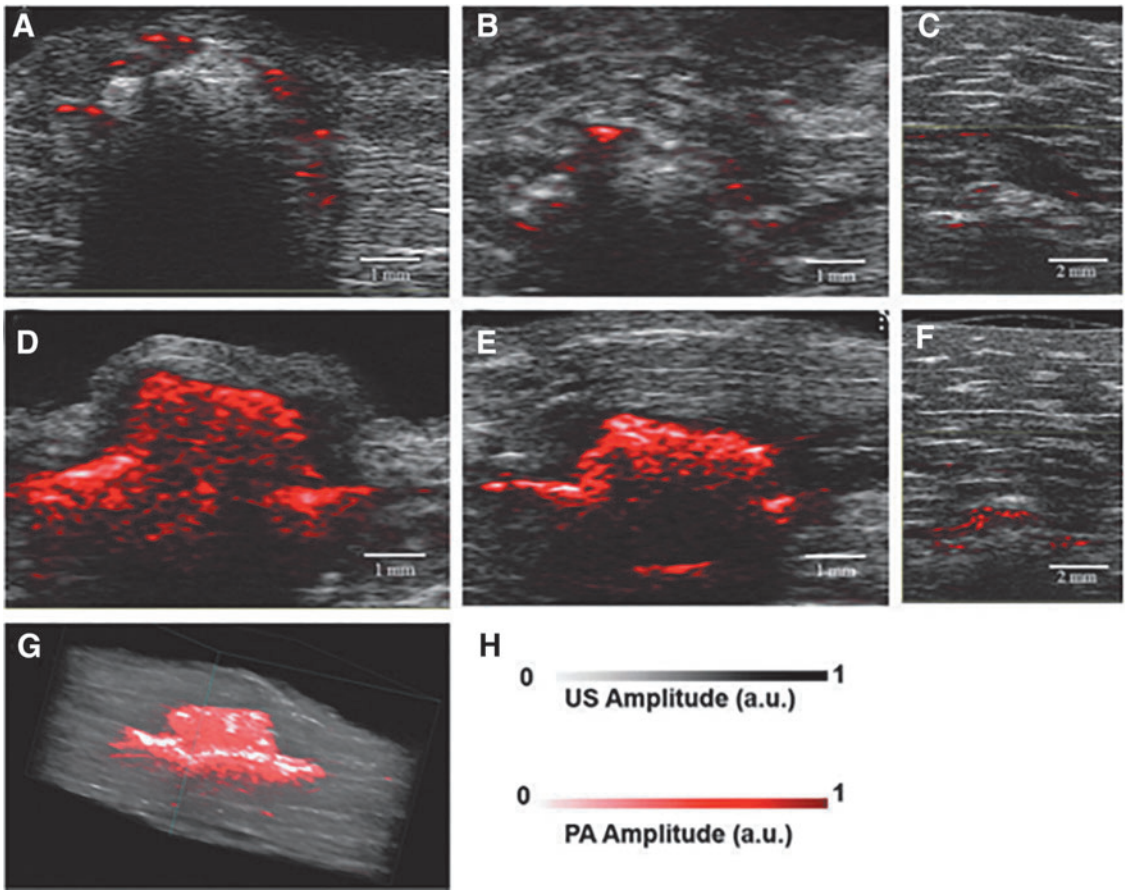

FIG. 4. PA imaging of scaffolds. US-PA images of PLGA **(A–C)** and SWNT-PLGA **(D–F)** scaffolds imaged at 680 nm embedded into chicken breast tissue at depths of **(A, D)** 0.5 mm **(B, E)** 2 mm and **(C, F)** 6 mm **(G)** 3D US-PA image rendition of SWNT-PLGA scaffolds embedded 0.5 mm in chicken breast tissue **(H)** US/PA amplitude scale is shown. © 2014 Reprinted with permission from Mary Ann Liebert.[113] 3D, three-dimensional; PLGA, poly(lactic-co-glycolic acid); US-PA, ultrasound-photoacoustic. Color images are available online.

maps) of the PLGA scaffolds and SWNT-PLGA scaffolds were obtained at day 7 and 14, which suggest that noninvasive long-term monitoring of scaffolds postimplantation is possible with PAI. The rate of scaffold degradation plays an important role in tissue engineering. While *in vitro* degradation studies are routine, evaluation of *in vivo* degradation is difficult. Recently, PAI has been used for noninvasive structural assessment of degradable polymers *in vivo* in parallel with US shear wave imaging for analysis of polymer mechanical properties.[114] The PAI signal from the scaffolds agreed with histological images obtained from the explanted tissue. This result indicates that PAI can be utilized to monitor structural changes that may occur in the scaffolds *in vivo*. PAI technique may provide vital information about tissue engineering scaffolds postimplantation and hence fill the gaps in understanding between *in vitro* and *in vivo* degradation behavior.

Vascular imaging

One of the most established applications of PAI is the analysis of vasculature in tissue.[115–120] This noninvasive and label-free vasculature imaging approach has been utilized to study existing disease conditions, monitor therapeutic progress, and diagnose clinical conditions. Vascular imaging with PA has been successfully used in diagnosis and assessment of cancer,[121–123] cardiovascular diseases,[124] microvascular abnormalities,[120,125,126] and superficial soft tissue damages.[127] Vascularization is crucial for engineering tissues of sufficient volume for clinical impact.[128–130] In the absence of adequate nutrients and oxygen, tissues can become hypoxic hindering tissue development and function. Assessing vascular development and function in engineered tissues *in vivo* is vital. Early detection of relevant abnormal vascularization condition may provide the opportunity to intervene to improve therapeutic outcomes or avoid catastrophic events.

Vascular imaging with PAI has been performed to evaluate wound healing. Wound healing involves three phases: Inflammation phase, proliferative phase, and remodeling and scar formation. The structural changes that occur following the inflammation phase include extracellular matrix formation, angiogenesis, granulation tissue formation, and reepithelialization.[131] PAI of angiogenesis and oxygen saturation level can be used to evaluate wound healing. A higher oxygen saturation level together with angiogenesis has been used as an indicator of wound healing and tissue regeneration.[132] In one study, PAI was used to monitor perfusion and hemodynamic changes in the burn healing process. PA images taken postburn at different interval demonstrated increased PA amplitude indicating neovascularization. The distribution and the density of neovascularization were qualitatively confirmed using histological analysis.[133] In another interesting application, PAI in combination with US imaging was first used to diagnose the severity of the burn and later used to track stem cells to monitor vascularization and skin tissue regeneration.[127] Three different temperatures (87°C, 100°C, and 133°C) for various durations were applied to mimic varying burn degrees. The PA images of the wound caused by 100°C and 113°C for 30 s indicated significant subcutaneous bleeding similar to third degree burns. No PA signal was observed in case of 87°C for 30 s and 113°C for 10 s indicating less severe burn injury. Skin incision verified PA images to be in well accordance with subcutaneous bleeding level suggesting that this technique can be used to determine the severity of burn injury. In a follow-up to this initial injury, PAI was used to monitor the therapeutic progress after treating burn injury with adipose-derived stem cells (ASCs). These ASCs were labeled with gold nanorods for imaging contrast. PA images were used to evaluate blood vessel density and blood perfusion at 2 weeks postinjury. Spectral PA images of ASCs and vascularization provided critical information regarding the morphological changes that occurred along the wound healing process (Fig. 5).

Recently, PAI was used to detect thrombosis in the carotid artery of a mouse model of ferric-chloride induced endothelial injury and arterial occlusive thrombus formation. Within thrombi, the hemoglobin concentration decreases. By measuring the optical absorption of hemoglobin, Li *et al.* reported the detection of artery thrombosis in mice.[134] Red blood cells (RBCs) in fresh clot formation generate higher PA signal than old clots. As the clot ages, it retracts forcing RBCs and other content out of the clot[135] resulting in a reduced PA signal. Based on this phenomenon, Karpiouk *et al.* used PAI to visualize thrombosis and estimate the age of the blood clot to differentiate the acute and the chronic stage of thrombosis.[136] While this application is not tissue engineering *per se*, the ability to evaluate clot formation could be useful in evaluating tissue-engineered vascular grafts. One recent study demonstrated PAI as a technique to monitor neovascularization and integration of decellularized human scaffold over an extended period of time postimplantation.[17] Decellularized scaffolds were implanted subcutaneously and monitored for neovascularization and integration over the period of 15 weeks. The higher PA signal intensity at 5 weeks indicated increased neovascularization, which plateaued at 12 and 15 weeks. The initial increase in PA signal intensity usually results from inflammatory effects; however, this effect lasts for a couple of days. A stable increase in PA intensity over the extended period could be attributed to neovascularization. Physically, the scaffolds retrieved after 15 weeks postimplantation were reported to integrate well. This study shows that we can leverage label-free imaging of vasculature to explore or test novel strategies to evaluate or improve the vascularization of bioengineered scaffolds or even organs using PAI.

PAI is a promising approach for vascular imaging and characterization due to its ability to achieve resolution in the range of 0.1–800 μm in the tissue thickness up to 8 cm all based on intrinsic contrast (Fig. 6A).[137] Furthermore, PAI of vascular function has been used to assess peripheral arterial disease (PAD).[138] PAD involves both large and small vessels. While large vessels are easily assessed using ultrasonography and CT angiography or MRI angiography, assessment of smaller vessels is hampered due to limited spatial resolution. PAI has been reported as a potential technique to evaluate small vessels-PAD. Detecting vascular changes induced in normal or diseased physiological conditions can provide crucial information relevant to PAD. To show changes in microvasculature circulation, the human index finger was subjected to the hot and cold stimulus to induce constriction and dilation of blood vessels (Fig. 6B). Stimulus induced changes in microcirculation were clearly

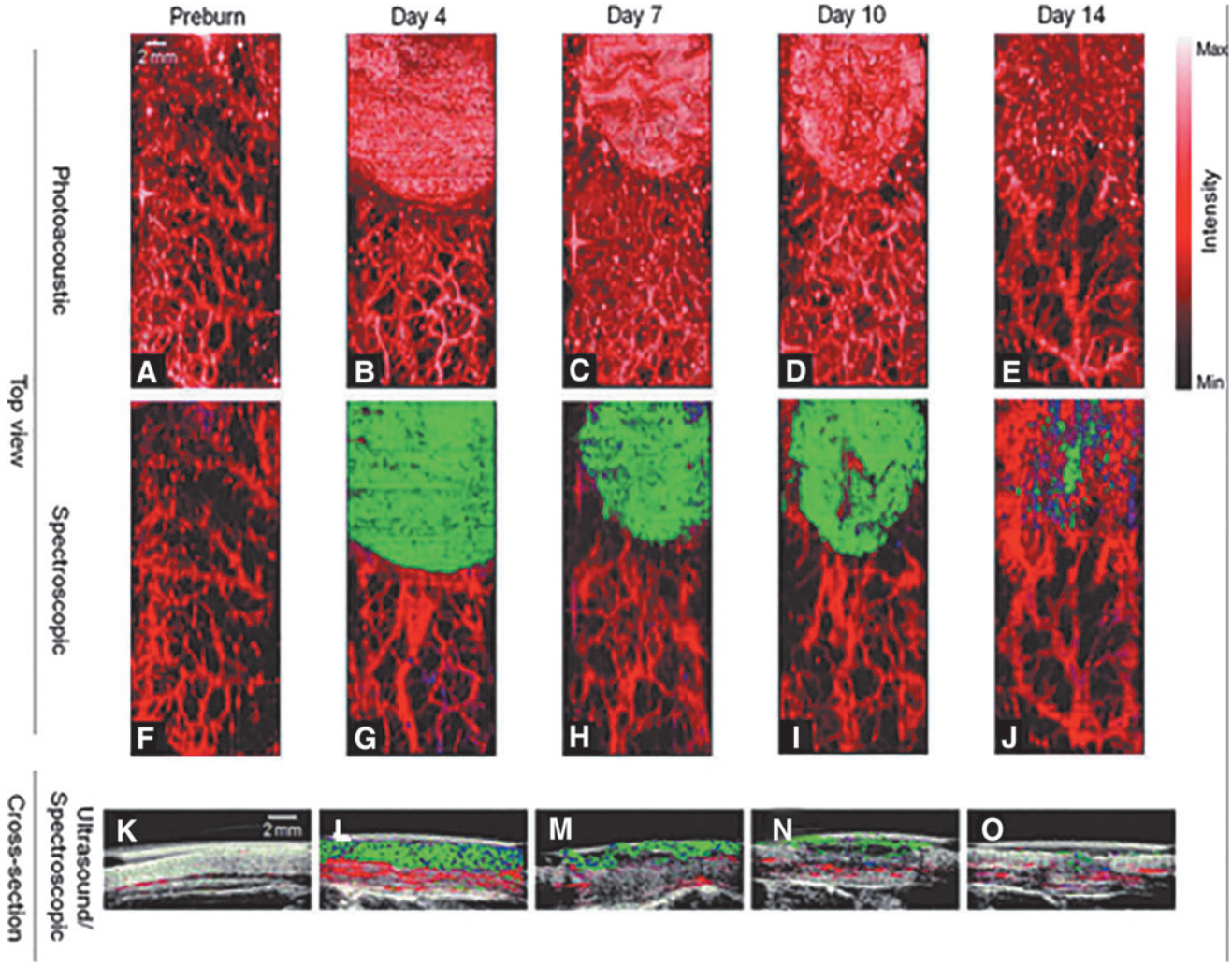

FIG. 5. PA imaging in cell tracking and monitoring. PA images of burn tissue treated with ASCs. ASCs were labeled with gold nanorods for PA contrast. Spectroscopic PA imaging allowed to identify and track ASCs over the period of 14 days. Oxygen saturation (oxygenated-*red* and deoxygenated-*blue*) indicated wound healing or tissue regeneration process. © Reprinted with permission of Mary Ann Liebert.[127] ASCs, adipose-derived stem cells. Color images are available online.

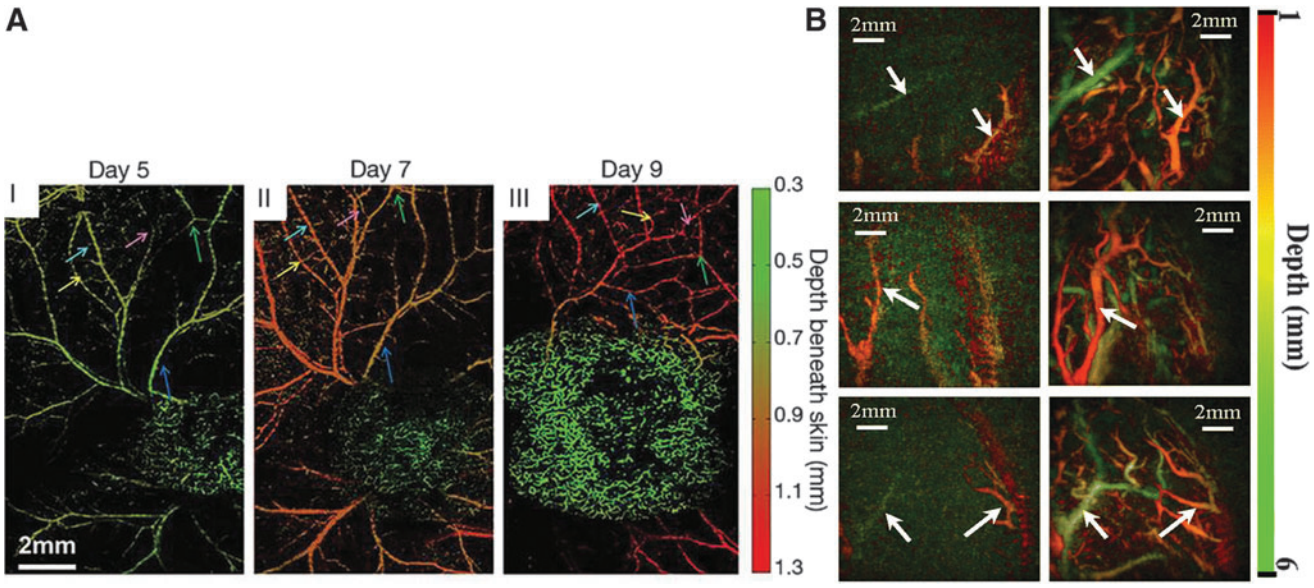

FIG. 6. **(A)** Label free imaging of angiogenesis at varying depths at different time points using PA imaging. © 2015 Reprinted with permission of AME.[137] **(B)** PA images of blood vessels after cold (*left*) and warm (*right*) stimulus. © 2018 Reprinted with permission of Springer Berlin Heidelberg.[138] Color images are available online.

visible in PA. This experiment represents a proof of concept for evaluating arterial diseases, including small vessels-PAD. The same technique can be used to test the results of strategies focused on increasing blood flow in peripheral vascular disease through the assessment of changes in vasculature circulation in response to a given stimulus.

Cell tracking and monitoring

Like polymers, cells also lack intrinsic cellular contrast except for melanoma cells. Melanin, a characteristic of melanoma cells, generates intrinsic PA contrast. Due to this intrinsic contrast of melanoma cells, Zhang *et al.* reported cell migration, distribution, and quantification of melanoma cells in PLGA scaffold for the first time.[139] PLGA scaffold did not generate PA contrast; however, spatial distribution and temporal proliferation of cells inside the 3D scaffold of thickness over 1 mm were visible with PAI. In the absence of intrinsic absorbance, external agents are used to generate PA contrast. One of the major external contrast applications in tissue engineering is cell tracking and monitoring.

Cells are often implanted as a critical component of a tissue regeneration strategy. One of the major challenges in stem cell therapy is tracking and monitoring of cells following implantation. This may provide vital information about the therapeutic outcome of the treatment, mechanism of the therapeutic effect, and potential risks of ectopic effects. It is crucial to understand cell fate, engraftment, and survival *in vivo* to understand the underlying mechanism of the stem cell function. PAI has been used as a noninvasive measure to track stem cells following implantation. To date, various contrast agents have been investigated for stem cell tracking, including dyes,[36,140] reporter genes,[141] fluorescent probes,[142] and NP.[143,144] Recently, bone mesenchymal stem cells (BMSCs) were investigated as a treatment in a mice brain injury model and were labeled with Prussian blue particles to generate PA image contrast.[36] PA tomography images following BMSC treatment provided pathophysiological status of brain injury, vascularization information, and recovery process. PA images indicated injury location and change in the bleeding area starting at 3 min following injury. There was dramatic increase in PA signal until 30 min postinjury; later, PA signal gradually decreased due to blood coagulation and spreading of blood pool and could no longer be detected on day 13 indicating the natural recovery process of about 15 days. Another study applied PAI to image and monitor cells implanted 6–8 mm deep in mice. In this study, a tyrosine based reporter gene was used to selectively label cells for long-term monitoring of cells.[145] With this technique, cells could be engineered to constitutively express tyrosinase (Tyr), an enzyme that catalyzes the formation of eumelanin, to provide PA contrast. Expression of the tyrosinase reporter allowed for monitoring of MSCs post transplantation in an acute myocardial infarction rat model.[146]

Gold labeled NPs have also been used to track cells. GNPs generate PA contrast that can be tuned based on NP size and structure. Nam *et al.* demonstrated *in vivo* imaging of GNP-labeled MSCs using PAI.[147] MSCs were prelabeled with GNPs and mixed with a PEGylated fibrin gel in 1:1 volume ratio and then injected intramuscularly at the tissue depth of $\sim$5 mm. They reported that GNP-labeled MSCs could be monitored for 10 days following injection. The same group previously reported that GNPs did not alter the cell viability, cell proliferation, or differentiation of MSCs suggesting that GNPs could be used for long-term monitoring of cells *in vivo*.[148,149] PAI has been used to evaluate endothelial cell distribution in decellularized scaffold during reendothelialization.[150] In another similar study, PAI was used to track and monitor GNP labeled ASCs for dermal tissue engineering. In this study, GNP labeled ASCs were detected up to 2 weeks in a PEG-based scaffold.[151] Furthermore, silica coating on GNPs as a contrast agent demonstrated enhanced PA in comparison with uncoated GNPs to track and monitor MSCs.[152,153] Similar to PEGylated GNPs, silica coating did not evoke any significant effect in the therapeutic effectiveness of stem cells. Jokerst *et al.* showed that silica coated GNPs did not affect the pluripotency of stem cells.[153] Further research is needed for assessing cell behavior and the immune response toward the silica coated GNPs.[154] Recently, PAI was used to guide the delivery of stem cells into the rodent spinal cord. GNP labeled MSCs were imaged in real time while being injected into the spinal cord of the rat. They report detecting cell number as low as 1000 cells with this imaging system.[155] In another study, human embryonic stem cell derived cardiomyocytes were delivered to the heart of the mouse for cardiac regenerative therapy. These cells were tagged with PA NPs that consist of semiconducting polymers, poly [2,6-(4,4-bis-(2-ethylhexyl)-4H-cyclopenta [2,1-b;3,4-b′]dithiophene)-alt-4,7(2,1,3 benzothiadia-zole)], for cell tracking and monitoring purpose. Strong PAI signals from these NPs easily differentiated implanted cells from background tissues.[156]

Current Status of PAI in Diagnostic Applications

Label-free detection of vascularization is one of the most appealing applications of PAI. Based on this and other advantages of multispectral PAI techniques have been developed for the evaluation and assessment of many disease states. Generally, these studies have exploited the ability of PAI to evaluate hemodynamic changes due to abnormal vessel assembly or function in these conditions. For example, hypervascularization and increased oxygen saturation are hallmarks of inflammation. Extensive vascularization co-occurring with low oxygen saturation may indicate tumor stage or progression.[157] As blood vessels are easily visualized with PAI system without the aid of external contrast agent, PAI holds great potential for clinical diagnostic applications. This includes cancer, cardiovascular disorders, inflammatory diseases, rheumatoid arthritis (RA), myocardial infarction, and diabetic retinopathy.[158] The research described in this section provides examples of PAI used in other medical applications using approaches that have not been fully exploited by researchers in the fields of TERM.

Inflammatory diseases

Increased vascularization and oxygen saturation often mark an inflammatory state.[159] In many instances, clinical outcomes of inflammatory disease treatments depend on early diagnosis and intervention.[160] Increased vascularization in arthritic joints of RA patients exhibited up to a 10-fold increase in the PA signal compared to noninflamed

joint.[161] In addition to diagnosis, PAI reportedly monitored the escalation of inflammation and the therapeutic effect of the treatment.[162,163] For example, in Crohn's disease (CD) chronic relapse of inflammation is common. A tool that allows quick detection of inflammation based on tissue perfusion and oxygenation allows for intervention or adjusting the treatment therapy. Although a detailed study is required, preliminary results performed in 108 patients suggest that PAI can be used to noninvasively evaluate CD based on hemoglobin levels in the intestinal wall.[164] In addition, CD may be characterized by fibrosis in addition to inflammation that is attributed by the irreversible deposition of collagen. CD fibrotic stricture may require surgical intervention, and therefore, accurate characterization of stricture is critical. Due to the optical absorbance of collagen around 1300 nm, PAI has shown to detect the presence of fibrotic stricture noninvasively in CD.[165]

Atherosclerosis is characterized by prolonged inflammation. The complex structure of vascular plaques correlates with disease progression and risk.[166] The plaque composition is important to access its rupture vulnerability and to determine the course of treatment. Intravascular PA (IVPA) imaging has been reported to allow differentiation between the various components within an atherosclerotic lesion.[56,167–169] IVPA utilizes a catheter or probe-based system for intravascular delivery of light to generate PA signal. The basis for detecting atherosclerotic plaque using PAI is the difference in optical absorbance of blood, collagen, and lipid.[170] The vulnerability of plaques can be evaluated in an atherosclerosis rabbit model by targeted macrophages with NPs.[171] However, the inherent challenge in IVPA is to design a flexible catheter or probe with clinically relevant diameter that has high sensitivity and chemical specificity.[58] Furthermore, these catheters or probes should have sufficient resolution to provide structural and functional information of the vascular wall. Many design considerations are currently being investigated to optimize IVPA catheter designs.[58,172,173] Nevertheless, PAI is a powerful tool for evaluating inflammation in a variety of disease states suggesting that it could be utilized to assess the response of a tissue to an implanted tissue engineering or biomaterial-based therapeutic.

Cancer

PAI in oncology is rapidly evolving. PAI is already in clinical trials for the detection of some types of cancers, while for many others it is in preclinical or investigational phase.[123,174–178] While a standardized technique is required for PAI before its transition to routine clinical use, the current in-house prototypes have demonstrated promising results for a wide range of cancers such as breast,[179–181] cervical,[182] prostate,[183] skin,[184] thyroid,[185] and ovarian cancer.[157] PAI leverages vasculature imaging and functional information such as oxygen saturation for cancer detection,[178] progression,[186] characterization,[187–191] prognosis, and monitoring therapeutic efficiency of treatment.[192–194] Delivery vehicles for cancer therapy are equipped with different PA contrast agents for multimodal imaging for better diagnosis and staging of cancer.[195] Neovascularization is commonly observed in tumors, triggered by the hypoxic state within the tissue.[196] Oxygen saturation level and extent of vascularization can be an indication of cancer progression. Longitudinal monitoring of vascular parameters gives insight into the therapeutic progress of a given treatment. In addition to the detection and characterization of cancer, PAI has also been used to stage cancer. When a primary tumor metastasizes, they first localize to a regional sentinel lymph node. With the aid of an external contrast agent, PAI has been used to noninvasively locate a sentinel lymph node to guide biopsy with minimal surgical procedures.[197]

Future Prospects

PAI offers several potential advantages of other imaging modalities when real-time longitudinal monitoring of functional imaging is needed. PAI does not use ionization energy allowing long term monitoring over the course of weeks or months. PAI allows tracking and monitoring of cells, as well as biomaterials, following implantation with the aid of external contrast agents. While PAI has seen heavy investigation in stem cell tracking, biomaterial monitoring is not well explored yet. One of the challenges in tissue engineering is monitoring *in vivo* degradation of scaffold.[3] Extrinsic contrast agents can be incorporated in the scaffolds or tissue engineering constructs to monitor and evaluate degradation behavior *in vivo*. Concomitant vasculature development can be imaged following scaffold implantation. Often after the surgical biomedical therapeutic intervention, there exists a risk of certain complication. Based on the amount of hemoglobin present at the injury site, it can be monitored to evaluate whether the injury is progressing toward wound healing route or inflammation route which would allow to better manage the clinical outcome of the therapeutic procedure.

There has been a recent upsurge in interest in PAI based on its strong potential for clinical imaging. However, several challenges still need to be addressed. The depth of tissue imaging can be increased but typically at the cost of resolution. Catheter or endoscopic PA probes are under development, which enable localized evaluation of specific internal organs or tissues while overcoming depth-related resolution issues. These tools may not be broadly applicable in TERM but certainly can be an important tool in specific applications such as tissue engineered vascular grafts. While there are many PA contrast agents under investigation, longitudinal monitoring could be improved through the development of contrast agents that provide sustained PA contrast. Most PA systems allow qualitative evaluation, and the development of more quantitative PA techniques will have a significant impact on biomedical research. Finally, the development of standardized, easy-to-use commercial systems will increase the impact of PAI.

Conclusions

There is a significant need for tools that allow monitoring and tracking of tissue engineering therapies. While there are many imaging strategies that are currently used to evaluate these processes, PAI offers an attractive alternative. The endogenous contrast resulting from vascularization, collagen, and lipids enables insight in the absence of any additional factors. In addition, given the wide range of available external contrast agents, PAI has immense potential to monitor specific characteristics such as cells or scaffolds by incorporating or targeting with exogenous agents. Monitoring

cell behavior or processes *in vivo* real time, therefore, can provide better understanding of how the given stimulus or biological process affects the cellular or therapeutic response in general. In addition, this information can be used as a feedback to design improved tissue engineering constructs for reconstruction, repair, or regenerative purpose.

Disclosure Statement

No competing financial interests exist.

Funding Information

Our work was supported by National Institute of Health (NIH) grants 5R01EB020604, 1R21EB008765, and R01NS102213, Cancer prevention and Research Institute of Texas (CPRIT) RP120558, and U.S. Department of Defense (DoD) W911NF-17-1-0488. This work was also supported by Research Initiative for Scientific Enhancement (RISE) R25GM060655.

References

1. Berthiaume, F., Maguire, T.J., and Yarmush, M.L. Tissue engineering and regenerative medicine: history, progress, and challenges. Ann Rev Chem Biomol Eng **2,** 403, 2011.
2. Mota, C., Puppi, D., Chiellini, F., and Chiellini, E. Additive manufacturing techniques for the production of tissue engineering constructs. J Tissue Eng Regen Med **9,** 174, 2015.
3. Appel, A.A., Anastasio, M.A., Larson, J.C., and Brey, E.M. Imaging challenges in biomaterials and tissue engineering. Biomaterials **34,** 6615, 2013.
4. Wang, L.V. Tutorial on photoacoustic microscopy and computed tomography. IEEE J Sel Top Quantum Electron **14,** 171, 2008.
5. Xu, M., and Wang, L.V. Photoacoustic imaging in biomedicine. Rev Sci Instrum **77,** 041101, 2006.
6. Beard, P. Biomedical photoacoustic imaging. Interface Focus. **1,** 602, 2011. Google Scholar 2011.
7. Cox, B.T., Laufer, J.G., Beard, P.C., and Arridge, S.R. Quantitative spectroscopic photoacoustic imaging: a review. J Biomed Opt **17,** 061202, 2012.
8. Wang, L.V., and Hu, S. Photoacoustic tomography: in vivo imaging from organelles to organs. Science **335,** 1458, 2012.
9. Wang, T., Wang, D., Yu, H., *et al.* Intracellularly acid-switchable multifunctional micelles for combinational photo/chemotherapy of the drug-resistant tumor. ACS Nano **10,** 3496, 2016.
10. Rosencwaig, A., and Gersho, A. Theory of the photoacoustic effect with solids. J Appl Phys **47,** 64, 1976.
11. Poudel, J., Lou, Y., and Anastasio, M.A. A survey of computational frameworks for solving the acoustic inverse problem in three-dimensional photoacoustic computed tomography. Phys Med Biol **64,** 14TR01, 2019.
12. Hillman, E.M., Amoozegar, C.B., Wang, T., *et al.* In vivo optical imaging and dynamic contrast methods for biomedical research. Philos Trans A Math Phys Eng Sci **369,** 4620, 2011.
13. Durr, N.J., Weisspfennig, C.T., Holfeld, B.A., and Ben-Yakar, A. Maximum imaging depth of two-photon autofluorescence microscopy in epithelial tissues. J Biomed Opt **16,** 026008, 2011.
14. Razansky, D., Vinegoni, C., and Ntziachristos, V. Multispectral photoacoustic imaging of fluorochromes in small animals. Optics Lett **32,** 2891, 2007.
15. Yao, J., and Wang, L.V. Photoacoustic tomography: fundamentals, advances and prospects. Contrast Media Mol Imaging **6,** 332, 2011.
16. Ogunlade, O., Ho, J.O., Kalber, T.L., *et al.* Monitoring neovascularization and integration of decellularized human scaffolds using photoacoustic imaging. Photoacoustics **13,** 76, 2019.
17. De Montigny, E. Photoacoustic tomography: principles and applications. Department of Physics Engineering, Polytechnic School Montreal 2011.
18. Wang, L.V. Photoacoustic Imaging and Spectroscopy. Boca Raton, FL: CRC Press, 2009.
19. Yao, D.-K., Zhang, C., Maslov, K.I., and Wang, L.V. Photoacoustic measurement of the Grüneisen parameter of tissue. J Biomed Opt **19,** 017007, 2014.
20. Balas, C. Review of biomedical optical imaging—a powerful, non-invasive, non-ionizing technology for improving in vivo diagnosis. Meas Sci Technol **20,** 104020, 2009.
21. Lin, L., Hu, P., Shi, J., *et al.* Single-breath-hold photoacoustic computed tomography of the breast. Nat Commun **9,** 2352, 2018.
22. Yao, J., Xia, J., and Wang, L.V. Multiscale functional and molecular photoacoustic tomography. Ultrason Imaging **38,** 44, 2016.
23. Xu, M., and Wang, L.V. Universal back-projection algorithm for photoacoustic computed tomography. Phys Rev E **71,** 016706, 2005.
24. Huang, H., Bustamante, G., Peterson, R., and Ye, J.Y. An adaptive filtered back-projection for photoacoustic image reconstruction. Med Phys **42,** 2169, 2015.
25. Rosenthal, A., Razansky, D., and Ntziachristos, V. Fast semi-analytical model-based acoustic inversion for quantitative optoacoustic tomography. IEEE Trans Med Imaging **29,** 1275, 2010.
26. Wang, K., Ermilov, S.A., Su, R., Brecht, H.-P., Oraevsky, A.A., and Anastasio, M.A. An imaging model incorporating ultrasonic transducer properties for three-dimensional optoacoustic tomography. IEEE Trans Med Imaging **30,** 203, 2010.
27. Wang, K., Su, R., Oraevsky, A.A., and Anastasio, M.A. Investigation of iterative image reconstruction in three-dimensional optoacoustic tomography. Phys Med Biol **57,** 5399, 2012.
28. Rosenthal, A., Jetzfellner, T., Razansky, D., and Ntziachristos, V. Efficient framework for model-based tomographic image reconstruction using wavelet packets. IEEE Trans Med Imaging **31,** 1346, 2012.
29. Frikel, J., and Haltmeier, M. Efficient regularization with wavelet sparsity constraints in photoacoustic tomography. Inverse Probl **34,** 024006, 2018.
30. Poudel, J., Matthews, T.P., Li, L., Anastasio, M.A., and Wang, L.V. Mitigation of artifacts due to isolated acoustic heterogeneities in photoacoustic computed tomography using a variable data truncation-based reconstruction method. J Biomed Opt **22,** 041018, 2017.
31. Matthews, T.P., Poudel, J., Li, L., Wang, L.V., and Anastasio, M.A. Parameterized joint reconstruction of the initial pressure and sound speed distributions for photoacoustic computed tomography. SIAM J Imaging Sci **11,** 1560, 2018.

32. Huang, C., Wang, K., Nie, L., Wang, L.V., and Anastasio, M.A. Full-wave iterative image reconstruction in photoacoustic tomography with acoustically inhomogeneous media. IEEE Trans Med Imaging **32,** 1097, 2013.
33. Poudel, J., Matthews, T.P., and Anastasio, M.A. Joint image reconstruction of initial pressure distribution and acoustic parameters in elastic media with application to transcranial photoacoustic tomography (Conference Presentation). In: Presented at the Medical Imaging 2018: Ultrasonic Imaging and Tomography. Bellingham, WA: SPIE Digital Library, 2018.
34. Mitsuhashi, K., Wang, L.V., and Anastasio, M.A. Image reconstruction in transcranial photoacoustic computed tomography of the brain. In: Presented at the Photons Plus Ultrasound: Imaging and Sensing 2015. Bellingham, WA: SPIE Digital Library, 2015.
35. Lutzweiler, C., and Razansky, D. Optoacoustic imaging and tomography: reconstruction approaches and outstanding challenges in image performance and quantification. Sensors (Basel) **13,** 7345, 2013.
36. Liu, W., and Yao, J. Photoacoustic microscopy: principles and biomedical applications. Biomed Eng Lett **8,** 203, 2018.
37. Yao, J., and Wang, L.V. Photoacoustic microscopy. Laser Photonics Rev **7,** 758, 2013.
38. Hu, S., Maslov, K., and Wang, L.V. Second-generation optical-resolution photoacoustic microscopy with improved sensitivity and speed. Opt Lett **36,** 1134, 2011.
39. Taruttis, A., and Ntziachristos, V. Advances in real-time multispectral optoacoustic imaging and its applications. Nat Photonics **9,** 219, 2015.
40. Keshava, N., and Mustard, J.F. Spectral unmixing. IEEE Signal Process Mag **19,** 44, 2002.
41. Tzoumas, S., and Ntziachristos, V. Spectral unmixing techniques for optoacoustic imaging of tissue pathophysiology. Philos Trans A Math Phys Eng Sci **375,** 20170262, 2017.
42. Bal, G., and Ren, K. On multi-spectral quantitative photoacoustic tomography in diffusive regime. Inverse Probl **28,** 025010, 2012.
43. Malone, E., Cox, B., and Arridge, S. Multispectral reconstruction methods for quantitative photoacoustic tomography. In: Presented at the Photons Plus Ultrasound: Imaging and Sensing 2016.
44. Taruttis, A., Timmermans, A.C., Wouters, P.C., Kacprowicz, M., van Dam, G.M., and Ntziachristos, V. Optoacoustic imaging of human vasculature: feasibility by using a handheld probe. Radiology **281,** 256, 2016.
45. Tzoumas, S., Nunes, A., Olefir, I., *et al.* Eigenspectra optoacoustic tomography achieves quantitative blood oxygenation imaging deep in tissues. Nat Commun **7,** 12121, 2016.
46. Stoffels, I., Morscher, S., Helfrich, I., *et al.* Metastatic status of sentinel lymph nodes in melanoma determined noninvasively with multispectral optoacoustic imaging. Sci Transl Med **7,** 317ra199, 2015.
47. Jansen, K., Wu, M., van der Steen, A.F., and van Soest, G. Lipid detection in atherosclerotic human coronaries by spectroscopic intravascular photoacoustic imaging. Opt Express **21,** 21472, 2013.
48. Burton, N.C., Patel, M., Morscher, S., *et al.* Multispectral opto-acoustic tomography (MSOT) of the brain and glioblastoma characterization. Neuroimage **65,** 522, 2013.
49. Yao, J., Maslov, K.I., Zhang, Y., Xia, Y., and Wang, L.V. Label-free oxygen-metabolic photoacoustic microscopy in vivo. J Biomed Opt **16,** 076003, 2011.
50. Hysi, E., Wirtzfeld, L.A., May, J.P., Undzys, E., Li, S.-D., and Kolios, M.C. Photoacoustic signal characterization of cancer treatment response: correlation with changes in tumor oxygenation. Photoacoustics **5,** 25, 2017.
51. Francis, M.E., Uriel, S., and Brey, E.M. Endothelial cell–matrix interactions in neovascularization. Tissue Eng Part B Rev **14,** 19, 2008.
52. Jiang, Y., Harrison, T., Ranasinghesagara, J.C., and Zemp, R.J. Photoacoustic and high-frequency power Doppler ultrasound biomicroscopy: a comparative study. J Biomed Opt **15,** 056008, 2010.
53. Pinter, S.Z., and Lacefield, J.C. Detectability of small blood vessels with high-frequency power Doppler and selection of wall filter cut-off velocity for microvascular imaging. Ultrasound Med Biol **35,** 1217, 2009.
54. Allen, T.J., Beard, P.C., Hall, A., Dhillon, A.P., and Owen, J.S. Spectroscopic photoacoustic imaging of lipid-rich plaques in the human aorta in the 740 to 1400 nm wavelength range. J Biomed Opt **17,** 061209, 2012.
55. Jansen, K., Van Der Steen, A.F., van Beusekom, H.M., Oosterhuis, J.W., and van Soest, G. Intravascular photoacoustic imaging of human coronary atherosclerosis. Opt Lett **36,** 597, 2011.
56. Zhang, J., Yang, S., Ji, X., Zhou, Q., and Xing, D. Characterization of lipid-rich aortic plaques by intravascular photoacoustic tomography: ex vivo and in vivo validation in a rabbit atherosclerosis model with histologic correlation. J Am Coll Cardiol **64,** 385, 2014.
57. Wang, P., Wang, H.W., Sturek, M., and Cheng, J.X. Bond-selective imaging of deep tissue through the optical window between 1600 and 1850 nm. J Biophotonics **5,** 25, 2012.
58. Cao, Y., Hui, J., Kole, A., *et al.* High-sensitivity intravascular photoacoustic imaging of lipid-laden plaque with a collinear catheter design. Sci Rep **6,** 25236, 2016.
59. Piao, Z., Ma, T., Li, J., *et al.* High speed intravascular photoacoustic imaging with fast optical parametric oscillator laser at 1.7 μm. Appl Phys Lett **107,** 083701, 2015.
60. Wang, P., Wang, P., Wang, H.-W., and Cheng, J.-X. Mapping lipid and collagen by multispectral photoacoustic imaging of chemical bond vibration. J Biomed Opt **17,** 096010, 2012.
61. Oh, J.-T., Li, M.-L., Zhang, H.F., Maslov, K., and Wang, L.V. Three-dimensional imaging of skin melanoma in vivo by dual-wavelength photoacoustic microscopy. J Biomed Opt **11,** 034032, 2006.
62. Staley, J., Grogan, P., Samadi, A.K., Cui, H., Cohen, M.S., and Yang, X. Growth of melanoma brain tumors monitored by photoacoustic microscopy. J Biomed Opt **15,** 040510, 2010.
63. Kirkpatrick, N.D., Hoying, J.B., Botting, S.K., Weiss, J.A., and Utzinger, U. In vitro model for endogenous optical signatures of collagen. J Biomed Opt **11,** 054021, 2006.
64. Taroni, P., Quarto, G., Pifferi, A., *et al.* Optical identification of subjects at high risk for developing breast cancer. J Biomed Opt **18,** 060507, 2013.
65. Kruizinga, P., van der Steen, A.F., de Jong, N., *et al.* Photoacoustic imaging of carotid artery atherosclerosis. J Biomed Opt **19,** 110504, 2014.
66. Wilson, R.H., Nadeau, K.P., Jaworski, F.B., Tromberg, B.J., and Durkin, A.J. Review of short-wave infrared spectroscopy and imaging methods for biological tissue characterization. J Biomed Opt **20,** 030901, 2015.

67. Sekar, S.K.V., Bargigia, I., Dalla Mora, A., *et al.* Diffuse optical characterization of collagen absorption from 500 to 1700 nm. J Biomed Opt **22,** 015006, 2017.
68. Weber, J., Beard, P.C., and Bohndiek, S.E. Contrast agents for molecular photoacoustic imaging. Nat Methods **13,** 639, 2016.
69. Yang, X., Stein, E.W., Ashkenazi, S., and Wang, L.V. Nanoparticles for photoacoustic imaging. Wiley Interdiscip Rev Nanomed Nanobiotechnol **1,** 360, 2009.
70. Wilson, K.E., Wang, T.Y., and Willmann, J.K. Acoustic and photoacoustic molecular imaging of cancer. J Nucl Med **54,** 1851, 2013.
71. Pansare, V.J., Hejazi, S., Faenza, W.J., and Prud'homme, R.K. Review of long-wavelength optical and NIR imaging materials: contrast agents, fluorophores, and multifunctional nano carriers. Chem Mater **24,** 812, 2012.
72. Mayerhöffer, U., Fimmel, B., and Würthner, F. Bright near-infrared fluorophores based on squaraines by unexpected halogen effects. Angew Chem Int Ed Engl **51,** 164, 2012.
73. Sreejith, S., Joseph, J., Lin, M., *et al.* Near-infrared squaraine dye encapsulated micelles for in vivo fluorescence and photoacoustic bimodal imaging. ACS Nano **9,** 5695, 2015.
74. Ntziachristos, V., and Razansky, D. Molecular imaging by means of multispectral optoacoustic tomography (MSOT). Chem Rev **110,** 2783, 2010.
75. Mishra, A., Jiang, Y., Roberts, S., Ntziachristos, V., and Westmeyer, G.G. Near-infrared photoacoustic imaging probe responsive to calcium. Anal Chem **88,** 10785, 2016.
76. Upadhyay, R. Role of calcium bio-minerals in regenerative medicine and tissue engineering. J Stem Cell Res Ther **2,** 00081, 2017.
77. Nakamura, S., Matsumoto, T., Sasaki, J.-I., *et al.* Effect of calcium ion concentrations on osteogenic differentiation and hematopoietic stem cell niche-related protein expression in osteoblasts. Tissue Eng Part A **16**, 2467, 2010.
78. Filonov, G.S., Piatkevich, K.D., Ting, L.-M., Zhang, J., Kim, K., and Verkhusha, V.V. Bright and stable near-infrared fluorescent protein for in vivo imaging. Nat Biotechnol **29,** 757, 2011.
79. Shcherbakova, D.M., and Verkhusha, V.V. Near-infrared fluorescent proteins for multicolor in vivo imaging. Nat Methods **10,** 751, 2013.
80. Shcherbakova, D.M., Baloban, M., Emelyanov, A.V., Brenowitz, M., Guo, P., and Verkhusha, V.V. Bright monomeric near-infrared fluorescent proteins as tags and biosensors for multiscale imaging. Nat Commun **7,** 12405, 2016.
81. Piatkevich, K.D., Suk, H.-J., Kodandaramaiah, S.B., *et al.* Near-infrared fluorescent proteins engineered from bacterial phytochromes in neuroimaging. Biophys J **113,** 2299, 2017.
82. Brunker, J., Yao, J., Laufer, J., and Bohndiek, S.E. Photoacoustic imaging using genetically encoded reporters: a review. J Biomed Opt **22,** 070901, 2017.
83. Willets, K.A., and Van Duyne, R.P. Localized surface plasmon resonance spectroscopy and sensing. Annu Rev Phys Chem **58,** 267, 2007.
84. Daniel, M.-C., and Astruc, D. Gold nanoparticles: assembly, supramolecular chemistry, quantum-size-related properties, and applications toward biology, catalysis, and nanotechnology. Chem Rev **104,** 293, 2004.
85. Chen, Y.-S., Frey, W., Kim, S., *et al.* Enhanced thermal stability of silica-coated gold nanorods for photoacoustic imaging and image-guided therapy. Opt Express **18,** 8867, 2010.
86. Chen, Y.-S., Frey, W., Kim, S., Kruizinga, P., Homan, K., and Emelianov, S. Silica-coated gold nanorods as photoacoustic signal nanoamplifiers. Nano Lett **11,** 348, 2011.
87. Segers, V.F., and Lee, R.T. Stem-cell therapy for cardiac disease. Nature **451,** 937, 2008.
88. Lindvall, O., Kokaia, Z., and Martinez-Serrano, A. Stem cell therapy for human neurodegenerative disorders-how to make it work. Nat Med **10,** S42, 2004.
89. De Coppi, P., Bartsch, G., Jr., Siddiqui, M.M., *et al.* Isolation of amniotic stem cell lines with potential for therapy. Nat Biotechnol **25,** 100, 2007.
90. Ankrum, J., and Karp, J.M. Mesenchymal stem cell therapy: two steps forward, one step back. Trends Mol Med **16,** 203, 2010.
91. Strauer, B.E., and Kornowski, R. Stem cell therapy in perspective. Circulation **107,** 929, 2003.
92. Ricles, L., Nam, S., Trevino, E., Emelianov, S., and Suggs, L. A dual gold nanoparticle system for mesenchymal stem cell tracking. J Mater Chem B **2,** 8220, 2014.
93. de la Zerda, A., Bodapati, S., Teed, R., *et al.* Family of enhanced photoacoustic imaging agents for high-sensitivity and multiplexing studies in living mice. ACS Nano **6,** 4694, 2012.
94. Liu, Z., Robinson, J.T., Sun, X., and Dai, H. PEGylated nanographene oxide for delivery of water-insoluble cancer drugs. J Am Chem Soc **130,** 10876, 2008.
95. Claveau, S., Bertrand, J.R., and Treussart, F. Fluorescent nanodiamond applications for cellular process sensing and cell tracking. Micromachines (Basel) **9,** 2018.
96. Zhang, B., Fang, C.-Y., Chang, C.-C., *et al.* Photoacoustic emission from fluorescent nanodiamonds enhanced with gold nanoparticles. Biomed Opt Express **3,** 1662, 2012.
97. Cai, X., Paratala, B.S., Hu, S., Sitharaman, B., and Wang, L.V. Multiscale photoacoustic microscopy of single-walled carbon nanotube-incorporated tissue engineering scaffolds. Tissue Eng Part C Methods **18,** 310, 2011.
98. Karageorgiou, V., and Kaplan, D. Porosity of 3D biomaterial scaffolds and osteogenesis. Biomaterials **26,** 5474, 2005.
99. Yin, C., Wen, G., Liu, C., *et al.* Organic semiconducting polymer nanoparticles for photoacoustic labeling and tracking of stem cells in the second near-infrared window. ACS Nano **12,** 12201, 2018.
100. Feng, L., Zhu, C., Yuan, H., Liu, L., Lv, F., and Wang, S. Conjugated polymer nanoparticles: preparation, properties, functionalization and biological applications. Chem Soc Rev **42,** 6620, 2013.
101. Gurtner, G.C., Werner, S., Barrandon, Y., and Longaker, M.T. Wound repair and regeneration. Nature **453,** 314, 2008.
102. Schneider, L.A., Korber, A., Grabbe, S., and Dissemond, J. Influence of pH on wound-healing: a new perspective for wound-therapy? Arch Dermatol Res **298,** 413, 2007.
103. Pu, K., Shuhendler, A.J., Jokerst, J.V., *et al.* Semiconducting polymer nanoparticles as photoacoustic molecular imaging probes in living mice. Nat Nanotechnol **9,** 233, 2014.
104. Lee, E.J., Kasper, F.K., and Mikos, A.G. Biomaterials for tissue engineering. Ann Biomed Eng **42,** 323, 2014.

105. Place, E.S., George, J.H., Williams, C.K., and Stevens, M.M. Synthetic polymer scaffolds for tissue engineering. Chem Soc Rev **38,** 1139, 2009.
106. Thiberge, S., Nechushtan, A., Sprinzak, D., *et al.* Scanning electron microscopy of cells and tissues under fully hydrated conditions. Proc Natl Acad Sci U S A **101,** 3346, 2004.
107. Dorsey, S.M., Lin-Gibson, S., and Simon C.G. Jr. X-ray microcomputed tomography for the measurement of cell adhesionand proliferation in polymer scaffolds. Biomaterials **30,** 2967, 2009.
108. Zhang, Y., Cai, X., Wang, Y., *et al.* Noninvasive photoacoustic microscopy of living cells in two and three dimensions through enhancement by a metabolite dye. Angew Chem Int Ed **50,** 7359, 2011.
109. Lu, W., Huang, Q., Ku, G., *et al.* Photoacoustic imaging of living mouse brain vasculature using hollow gold nanospheres. Biomaterials **31,** 2617, 2010.
110. Moon, H., Kumar, D., Kim, H., *et al.* Amplified photoacoustic performance and enhanced photothermal stability of reduced graphene oxide coated gold nanorods for sensitive photoacoustic imaging. ACS Nano **9,** 2711, 2015.
111. Lalwani, G., Cai, X., Nie, L., Wang, L.V., and Sitharaman, B. Graphene-based contrast agents for photoacoustic and thermoacoustic tomography. Photoacoustics **1,** 62, 2013.
112. Cai, X., Zhang, Y., Li, L., *et al.* Investigation of neovascularization in three-dimensional porous scaffolds in vivo by a combination of multiscale photoacoustic microscopy and optical coherence tomography. Tissue Eng Part C Methods **19,** 196, 2012.
113. Talukdar, Y., Avti, P., Sun, J., and Sitharaman, B. Multimodal ultrasound-photoacoustic imaging of tissue engineering scaffolds and blood oxygen saturation in and around the scaffolds. Tissue Eng Part C Methods **20,** 440, 2014.
114. Park, D.W., Ye, S.-H., Jiang, H.B., *et al.* In vivo monitoring of structural and mechanical changes of tissue scaffolds by multi-modality imaging. Biomaterials **35,** 7851, 2014.
115. Zhang, E., Laufer, J., Pedley, R., and Beard, P. In vivo high-resolution 3D photoacoustic imaging of superficial vascular anatomy. Phys Med Biol **54,** 1035, 2009.
116. Ku, G., Wang, X., Xie, X., Stoica, G., and Wang, L.V. Imaging of tumor angiogenesis in rat brains in vivo by photoacoustic tomography. Appl Opt **44,** 770, 2005.
117. Hu, S., and Wang, L.V. Photoacoustic imaging and characterization of the microvasculature. J Biomed Opt **15,** 011101, 2010.
118. Xie, Z., Roberts, W., Carson, P., Liu, X., Tao, C., and Wang, X. Evaluation of bladder microvasculature with high-resolution photoacoustic imaging. Opt Lett **36,** 4815, 2011.
119. Pan, D., Pramanik, M., Senpan, A., *et al.* Molecular photoacoustic imaging of angiogenesis with integrin-targeted gold nanobeacons. FASEB J **25,** 875, 2011.
120. Gessner, R.C., Frederick, C.B., Foster, F.S., and Dayton, P.A. Acoustic angiography: a new imaging modality for assessing microvasculature architecture. J Biomed Imaging **2013,** 14, 2013.
121. Zhang, Q., Iwakuma, N., Sharma, P., *et al.* Gold nanoparticles as a contrast agent for in vivo tumor imaging with photoacoustic tomography. Nanotechnology **20,** 395102, 2009.
122. Lao, Y., Xing, D., Yang, S., and Xiang, L. Noninvasive photoacoustic imaging of the developing vasculature during early tumor growth. Phys Med Biol **53,** 4203, 2008.
123. Mallidi, S., Luke, G.P., and Emelianov, S. Photoacoustic imaging in cancer detection, diagnosis, and treatment guidance. Trends Biotechnol **29,** 213, 2011.
124. Al Mukaddim, R., Rodgers, A., Hacker, T.A., Heinmiller, A., and Varghese, T. Real-time in vivo photoacoustic imaging in the assessment of myocardial dynamics in murine model of myocardial ischemia. Ultrasound Med Biol **44,** 2155, 2018.
125. Okumura, K., Yoshida, K., Yoshioka, K., *et al.* Photoacoustic imaging of tumour vascular permeability with indocyanine green in a mouse model. Eur Radiol experimental **2,** 5, 2018.
126. Eisenbrey, J.R., Stanczak, M., Forsberg, F., Mendoza-Ballesteros, F.A., and Lyshchik, A. Photoacoustic oxygenation quantification in patients with Raynaud's: first-in-human results. Ultrasound Med Biol **44,** 2081, 2018.
127. Nam, S.Y., Chung, E., Suggs, L.J., and Emelianov, S.Y. Combined ultrasound and photoacoustic imaging to noninvasively assess burn injury and selectively monitor a regenerative tissue-engineered construct. Tissue Eng Part C Methods **21,** 557, 2015.
128. Rouwkema, J., Rivron, N.C., and van Blitterswijk, C.A. Vascularization in tissue engineering. Trends Biotechnol **26,** 434, 2008.
129. Rouwkema, J., and Khademhosseini, A. Vascularization and angiogenesis in tissue engineering: beyond creating static networks. Trends Biotechnol **34,** 733, 2016.
130. Papavasiliou, G., Cheng, M.-H., and Brey, E.M. Strategies for Vascularization of Polymer Scaffolds. London, United Kingdom: BMJ Publishing Group Limited, 2010.
131. Enoch, S., and Leaper, D.J. Basic science of wound healing. Surgery (Oxford) **26,** 31, 2008.
132. Tandara, A.A., and Mustoe, T.A. Oxygen in wound healing—more than a nutrient. World J Surg **28,** 294, 2004.
133. Aizawa, K., Sato, S., Saitoh, D., Ashida, H., and Obara, M. Photoacoustic monitoring of burn healing process in rats. J Biomed Opt **13,** 064020, 2008.
134. Li, B., Fu, C., Ma, G., Fan, Q., and Yao, Y. Photoacoustic imaging: a novel tool for detecting carotid artery thrombosis in mice. J Vasc Res **54,** 217, 2017.
135. Fineschi, V., Turillazzi, E., Neri, M., Pomara, C., and Riezzo, I. Histological age determination of venous thrombosis: a neglected forensic task in fatal pulmonary thrombo-embolism. Forensic Sci Int **186,** 22, 2009.
136. Karpiouk, A.B., Aglyamov, S.R., Mallidi, S., *et al.* Combined ultrasound and photoacoustic imaging to detect and stage deep vein thrombosis: phantom and ex vivo studies. J Biomed Opt **13,** 054061, 2008.
137. Lin, R., Chen, J., Wang, H., Yan, M., Zheng, W., and Song, L. Longitudinal label-free optical-resolution photoacoustic microscopy of tumor angiogenesis in vivo. Quant Imaging Med Surg **5,** 23, 2015.
138. Plumb, A.A., Huynh, N.T., Guggenheim, J., Zhang, E., and Beard, P. Rapid volumetric photoacoustic tomographic imaging with a Fabry-Perot ultrasound sensor depicts peripheral arteries and microvascular vasomotor responses to thermal stimuli. Eur Radiol **28,** 1037, 2018.
139. Zhang, Y., Cai, X., Choi, S.-W., Kim, C., Wang, L.V., and Xia, Y. Chronic label-free volumetric photoacoustic mi-

croscopy of melanoma cells in three-dimensional porous scaffolds. Biomaterials **31,** 8651, 2010.
140. Zheng, S., Li, H., Lai, K., *et al.* Noninvasive photoacoustic and fluorescent tracking of optical dye labeled T cellular activities of diseased sites at new depth. J Biophotonics e201800073, 2018.
141. Deán-Ben, X.L., Sela, G., Lauri, A., *et al.* Functional optoacoustic neuro-tomography for scalable whole-brain monitoring of calcium indicators. Light Sci Appl **5,** e16201, 2016.
142. Yao, J., Kaberniuk, A.A., Li, L., *et al.* Multiscale photoacoustic tomography using reversibly switchable bacterial phytochrome as a near-infrared photochromic probe. Nat Methods **13,** 67, 2016.
143. Lu, M., Cheng, X., Jiang, J., *et al.* Dual-modal photoacoustic and magnetic resonance tracking of tendon stem cells with PLGA/iron oxide microparticles in vitro. PLoS One **13,** e0193362, 2018.
144. Lyu, Y., Fang, Y., Miao, Q., Zhen, X., Ding, D., and Pu, K. Intraparticle molecular orbital engineering of semiconducting polymer nanoparticles as amplified theranostics for in vivo photoacoustic imaging and photothermal therapy. ACS Nano **10,** 4472, 2016.
145. Jathoul, A.P., Laufer, J., Ogunlade, O., *et al.* Deep in vivo photoacoustic imaging of mammalian tissues using a tyrosinase-based genetic reporter. Nat Photonics **9,** 239, 2015.
146. Liu, M., Wang, Y., Li, M., *et al.* Using tyrosinase as a trimodality reporter gene to monitor transplanted stem cells in acute myocardial infarction. Exp Mol Med **50,** 2018.
147. Nam, S.Y., Ricles, L.M., Suggs, L.J., and Emelianov, S.Y. In vivo ultrasound and photoacoustic monitoring of mesenchymal stem cells labeled with gold nanotracers. PLoS One **7,** e37267, 2012.
148. Ricles, L.M., Nam, S.Y., Sokolov, K., Emelianov, S.Y., and Suggs, L.J. Function of mesenchymal stem cells following loading of gold nanotracers. Int J Nanomed **6,** 407, 2011.
149. Meir, R., Motiei, M., and Popovtzer, R. Gold nanoparticles for in vivo cell tracking. Nanomedicine **9,** 2059, 2014.
150. Nagao, R.J., Ouyang, Y., Keller, R., *et al.* Ultrasound-guided photoacoustic imaging-directed re-endothelialization of acellular vasculature leads to improved vascular performance. Acta Biomater **32,** 35, 2016.
151. Chung, E., Nam, S.Y., Ricles, L.M., Emelianov, S.Y., and Suggs, L.J. Evaluation of gold nanotracers to track adipose-derived stem cells in a PEGylated fibrin gel for dermal tissue engineering applications. International journal of nanomedicine **8,** 325, 2013.
152. Nam, S.Y., Ricles, L.M., Suggs, L.J., and Emelianov, S.Y. Nonlinear photoacoustic signal increase from endocytosis of gold nanoparticles. Opt Lett **37,** 4708, 2012.
153. Jokerst, J.V., Thangaraj, M., Kempen, P.J., Sinclair, R., and Gambhir, S.S. Photoacoustic imaging of mesenchymal stem cells in living mice via silica-coated gold nanorods. ACS Nano **6,** 5920, 2012.
154. Tanaka, T., Narazaki, M., and Kishimoto, T. IL-6 in inflammation, immunity, and disease. Cold Spring Harb Perspect Biol **6,** a016295, 2014.
155. Donnelly, E.M., Kubelick, K.P., Dumani, D.S., and Emelianov, S.Y. Photoacoustic image-guided delivery of plasmonic-nanoparticle-labeled mesenchymal stem cells to the spinal cord. Nano Lett **18,** 6625, 2018.
156. Qin, X., Chen, H., Yang, H., *et al.* Photoacoustic imaging of embryonic stem cell-derived cardiomyocytes in living hearts with ultrasensitive semiconducting polymer nanoparticles. Adv Funct Mater **28,** 1704939, 2018.
157. Nandy, S., Mostafa, A., Hagemann, I.S., *et al.* Evaluation of ovarian cancer: initial application of coregistered photoacoustic tomography and US. Radiology **289,** 740, 2018.
158. Furuya, M., Nishiyama, M., Kasuya, Y., Kimura, S., and Ishikura, H. Pathophysiology of tumor neovascularization. Vasc Health Risk Manage **1,** 277, 2005.
159. Waldner, M.J., Knieling, F., Egger, C., *et al.* Multispectral optoacoustic tomography in Crohn's disease: noninvasive imaging of disease activity. Gastroenterology **151,** 238, 2016.
160. Jo, J., Tian, C., Xu, G., *et al.* Photoacoustic tomography for human musculoskeletal imaging and inflammatory arthritis detection. Photoacoustics **12,** 82, 2018.
161. van den Berg, P.J., Daoudi, K., Moens, H.J.B., and Steenbergen, W. Feasibility of photoacoustic/ultrasound imaging of synovitis in finger joints using a point-of-care system. Photoacoustics **8,** 8, 2017.
162. Rajian, J.R., Shao, X., Chamberland, D.L., and Wang, X. Characterization and treatment monitoring of inflammatory arthritis by photoacoustic imaging: a study on adjuvant-induced arthritis rat model. Biomed Opt Express **4,** 900, 2013.
163. Beziere, N., Von Schacky, C., Kosanke, Y., *et al.* Optoacoustic imaging and staging of inflammation in a murine model of arthritis. Arthritis Rheumatol **66,** 2071, 2014.
164. Knieling, F., Neufert, C., Hartmann, A., *et al.* Multispectral optoacoustic tomography for assessment of Crohn's disease activity. N Engl J Med **376,** 1292, 2017.
165. Lei, H., Johnson, L.A., Liu, S., *et al.* Characterizing intestinal inflammation and fibrosis in Crohn's disease by photoacoustic imaging: feasibility study. Biomed Opt Express **7,** 2837, 2016.
166. Appel, A., Chou, C., Larson, J., *et al.* An initial evaluation of analyser-based phase-contrast X-ray imaging of carotid plaque microstructure. Br J Radiol **86,** 20120318, 2013.
167. Sethuraman, S., Amirian, J.H., Litovsky, S.H., Smalling, R.W., and Emelianov, S.Y. Spectroscopic intravascular photoacoustic imaging to differentiate atherosclerotic plaques. Opt Express **16,** 3362, 2008.
168. Jansen, K., van Soest, G., and van der Steen, A.F. Intravascular photoacoustic imaging: a new tool for vulnerable plaque identification. Ultrasound Med Biol **40,** 1037, 2014.
169. Jansen, K., Wu, M., van der Steen, A.F., and van Soest, G. Photoacoustic imaging of human coronary atherosclerosis in two spectral bands. Photoacoustics **2,** 12, 2014.
170. Wu, M., Jansen, K., van der Steen, A.F., and van Soest, G. Specific imaging of atherosclerotic plaque lipids with two-wavelength intravascular photoacoustics. Biomed Opt Express **6,** 3276, 2015.
171. Qin, H., Zhao, Y., Zhang, J., Pan, X., Yang, S., and Xing, D. Inflammation-targeted gold nanorods for intravascular photoacoustic imaging detection of matrix metalloproteinase-2 (MMP2) in atherosclerotic plaques. Nanomed **12,** 1765, 2016.
172. Karpiouk, A.B., Wang, B., and Emelianov, S.Y. Development of a catheter for combined intravascular ultrasound and photoacoustic imaging. Rev Sci Instrum **81,** 014901, 2010.

173. Li, Y., Gong, X., Liu, C., *et al.* High-speed intravascular spectroscopic photoacoustic imaging at 1000 A-lines per second with a 0.9-mm diameter catheter. J Biomed Opt **20,** 065006, 2015.
174. Valluru, K.S., Wilson, K.E., and Willmann, J.K. Photoacoustic Imaging in oncology: translational preclinical and early clinical experience. Radiology **280,** 332, 2016.
175. Kitai, T., Torii, M., Sugie, T., *et al.* Photoacoustic mammography: initial clinical results. Breast Cancer **21,** 146, 2014.
176. Fakhrejahani, E., Torii, M., Kitai, T., *et al.* Clinical report on the first prototype of a photoacoustic tomography system with dual illumination for breast cancer imaging. PLoS One **10,** e0139113, 2015.
177. Valluru, K.S., and Willmann, J.K. Clinical photoacoustic imaging of cancer. Ultrasonography **35,** 267, 2016.
178. Toi, M., Asao, Y., Matsumoto, Y., *et al.* Visualization of tumor-related blood vessels in human breast by photoacoustic imaging system with a hemispherical detector array. Sci Rep **7,** 41970, 2017.
179. Ermilov, S.A., Khamapirad, T., Conjusteau, A., *et al.* Laser optoacoustic imaging system for detection of breast cancer. J Biomed Opt **14,** 024007, 2009.
180. Oraevsky, A., Clingman, B., Zalev, J., Stavros, A., Yang, W., and Parikh, J. Clinical optoacoustic imaging combined with ultrasound for coregistered functional and anatomical mapping of breast tumors. Photoacoustics **12,** 30, 2018.
181. Heijblom, M., Piras, D., van den Engh, F.M., *et al.* The state of the art in breast imaging using the Twente Photoacoustic Mammoscope: results from 31 measurements on malignancies. Eur Radiol **26,** 3874, 2016.
182. Peng, K., He, L., Wang, B., and Xiao, J. Detection of cervical cancer based on photoacoustic imaging—the in-vitro results. Biomed Opt Express **6,** 135, 2015.
183. Dogra, V.S., Chinni, B.K., Valluru, K.S., *et al.* Multispectral photoacoustic imaging of prostate cancer: preliminary ex-vivo results. J Clin Imaging Sci **3,** 2013.
184. Attia, A.B.E., Chuah, S.Y., Razansky, D., *et al.* Noninvasive real-time characterization of non-melanoma skin cancers with handheld optoacoustic probes. Photoacoustics **7,** 20, 2017.
185. Yang, M., Zhao, L., He, X., *et al.* Photoacoustic/ultrasound dual imaging of human thyroid cancers: an initial clinical study. Biomed Opt Express **8,** 3449, 2017.
186. Comenge, J., Sharkey, J., Fragueiro, O., *et al.* Multimodal cell tracking from systemic administration to tumour growth by combining gold nanorods and reporter genes. Elife **7,** e33140, 2018.
187. Yamaga, I., Kawaguchi-Sakita, N., Asao, Y., *et al.* Vascular branching point counts using photoacoustic imaging in the superficial layer of the breast: a potential biomarker for breast cancer. Photoacoustics **11,** 6, 2018.
188. Bar-Zion, A., Yin, M., Adam, D., and Foster, F.S. Functional flow patterns and static blood pooling in tumors revealed by combined contrast-enhanced ultrasound and photoacoustic imaging. Cancer Res **76,** 4320, 2016.
189. Balasundaram, G., Ho, C.J.H., Li, K., *et al.* Molecular photoacoustic imaging of breast cancer using an actively targeted conjugated polymer. Int J Nanomed **10,** 387, 2015.
190. Wilson, K.E., Bachawal, S.V., Abou-Elkacem, L., *et al.* Spectroscopic photoacoustic molecular imaging of breast cancer using a B7-H3-targeted ICG contrast agent. Theranostics **7,** 1463, 2017.
191. Mallidi, S., Kim, S., Karpiouk, A., Joshi, P.P., Sokolov, K., and Emelianov, S. Visualization of molecular composition and functionality of cancer cells using nanoparticle-augmented ultrasound-guided photoacoustics. Photoacoustics **3,** 26, 2015.
192. Mallidi, S., Watanabe, K., Timerman, D., Schoenfeld, D., and Hasan, T. Prediction of tumor recurrence and therapy monitoring using ultrasound-guided photoacoustic imaging. Theranostics **5,** 289, 2015.
193. Gerling, M., Zhao, Y., Nania, S., *et al.* Real-time assessment of tissue hypoxia in vivo with combined photoacoustics and high-frequency ultrasound. Theranostics **4,** 604, 2014.
194. Rich, L.J., and Seshadri, M. Photoacoustic imaging of vascular hemodynamics: validation with blood oxygenation level-dependent MR imaging. Radiology **275,** 110, 2014.
195. Shrestha, B., Tang, L., and Romero, G. Nanoparticles-mediated combination therapies for cancer treatment. Adv Ther **2,** 1900076, 2019.
196. Muz, B., de la Puente, P., Azab, F., and Azab, A.K. The role of hypoxia in cancer progression, angiogenesis, metastasis, and resistance to therapy. Hypoxia **3,** 83, 2015.
197. Garcia-Uribe, A., Erpelding, T.N., Krumholz, A., *et al.* Dual-modality photoacoustic and ultrasound imaging system for noninvasive sentinel lymph node detection in patients with breast cancer. Sci Rep **5,** 15748, 2015.
198. Li, W., Abram, F., Beaudoin, G., Berthiaume, M.-J., Pelletier, J.-P., and Martel-Pelletier, J. Human hip joint cartilage: MRI quantitative thickness and volume measurements discriminating acetabulum and femoral head. IEEE Trans Biomed Eng **55,** 2731, 2008.
199. Chen, Y.-C.I., Cypess, A.M., Chen, Y.-C., *et al.* Measurement of human brown adipose tissue volume and activity using anatomical MRI and functional MRI. J Nucl Med **54,** 1584, 2013.
200. Zhang, M., Liu, X., Huang, J., *et al.* Ultrasmall graphene oxide based T_1 MRI contrast agent for in vitro and in vivo labeling of human mesenchymal stem cells. Nanomedicine **14,** 2475, 2018.
201. Liu, Y., Liu, Y., Zheng, C., *et al.* Ru Nanoparticles coated with γ-Fe_2O_3 promoting and monitoring the differentiation of human mesenchymal stem cells via MRI tracking. Colloids Surf B Biointerfaces **170,** 701, 2018.
202. Bull, E., Madani, S.Y., Sheth, R., Seifalian, A., Green, M., and Seifalian, A.M. Stem cell tracking using iron oxide nanoparticles. Int J Nanomed **9,** 1641, 2014.
203. Andreas, K., Georgieva, R., Ladwig, M., *et al.* Highly efficient magnetic stem cell labeling with citrate-coated superparamagnetic iron oxide nanoparticles for MRI tracking. Biomaterials **33,** 4515, 2012.
204. Li, L., Jiang, W., Luo, K., *et al.* Superparamagnetic iron oxide nanoparticles as MRI contrast agents for non-invasive stem cell labeling and tracking. Theranostics **3,** 595, 2013.
205. Wei, H., Bruns, O.T., Kaul, M.G., *et al.* Exceedingly small iron oxide nanoparticles as positive MRI contrast agents. Proc Natl Acad Sci U S A **114,** 2325, 2017.
206. Majumdar, S., Pothirajan, P., Dorcemus, D., Nukavarapu, S., and Kotecha, M. High field sodium MRI assessment of stem cell chondrogenesis in a tissue-engineered matrix. Ann Biomed Eng **44,** 1120, 2016.
207. Ganesh, N., Ashokan, A., Rajeshkannan, R., Chennazhi, K., Koyakutty, M., and Nair, S.V. Magnetic resonance functional nano-hydroxyapatite incorporated poly (capro-

lactone) composite scaffolds for in situ monitoring of bone tissue regeneration by MRI. Tissue Eng Part A **20,** 2783, 2014.
208. Beaumont, M., DuVal, M.G., Loai, Y., Farhat, W.A., Sandor, G.K., and Cheng, H.L.M. Monitoring angiogenesis in soft-tissue engineered constructs for calvarium bone regeneration: an in vivo longitudinal DCE-MRI study. NMR Biomed **23,** 48, 2010.
209. Ceelen, W., Smeets, P., Backes, W., *et al.* Noninvasive monitoring of radiotherapy-induced microvascular changes using dynamic contrast enhanced magnetic resonance imaging (DCE-MRI) in a colorectal tumor model. Int J Radiat Oncol Biol Phys **64,** 1188, 2006.
210. Rauscher, A., Sedlacik, J., Barth, M., Haacke, E.M., and Reichenbach, J.R. Nonnvasive assessment of vascular architecture and function during modulated blood oxygenation using susceptibility weighted magnetic resonance imaging. Magn Reson Med **54,** 87, 2005.
211. Chaimow, D., Yacoub, E., Uğurbil, K., and Shmuel, A. Spatial specificity of the functional MRI blood oxygenation response relative to neuronal activity. Neuroimage **164,** 32, 2018.
212. Jerome, N.P., Hekmatyar, S.K., and Kauppinen, R.A. Blood oxygenation level dependent, blood volume, and blood flow responses to carbogen and hypoxic hypoxia in 9L rat gliomas as measured by MRI. J Magn Reson Imaging **39,** 110, 2014.
213. Martín-Badosa, E., Amblard, D., Nuzzo, S., Elmoutaouakkil, A., Vico, L., and Peyrin, F. Excised bone structures in mice: imaging at three-dimensional synchrotron radiation micro CT. Radiology **229,** 921, 2003.
214. Guldberg, R.E., Duvall, C.L., Peister, A., *et al.* 3D imaging of tissue integration with porous biomaterials. Biomaterials **29,** 3757, 2008.
215. Barbetta, A., Bedini, R., Pecci, R., and Dentini, M. Role of X-ray microtomography in tissue engineering. Ann Ist Super Sanita **48,** 10, 2012.
216. Bivard, A., Levi, C., Krishnamurthy, V., *et al.* Perfusion computed tomography to assist decision making for stroke thrombolysis. Brain **138,** 1919, 2015.
217. Arkudas, A., Beier, J.P., Pryymachuk, G., *et al.* Automatic quantitative micro-computed tomography evaluation of angiogenesis in an axially vascularized tissue-engineered bone construct. Tissue Eng Part C Methods **16,** 1503, 2010.
218. Young, S., Kretlow, J.D., Nguyen, C., *et al.* Microcomputed tomography characterization of neovascularization in bone tissue engineering applications. Tissue Eng Part B Re **14,** 295, 2008.
219. van Lenthe, G.H., Hagenmüller, H., Bohner, M., Hollister, S.J., Meinel, L., and Müller, R. Nondestructive microcomputed tomography for biological imaging and quantification of scaffold–bone interaction in vivo. Biomaterials **28,** 2479, 2007.
220. Cengiz, I.F., Oliveira, J.M., and Reis, R.L. Micro-computed tomography characterization of tissue engineering scaffolds: effects of pixel size and rotation step. J Mater Sci Mater Med **28,** 129, 2017.
221. Takashima, K., Hoshino, M., Uesugi, K., *et al.* X-ray phase-contrast computed tomography visualizes the microstructure and degradation profile of implanted biodegradable scaffolds after spinal cord injury. J Synchrotron Radiat **22,** 136, 2015.
222. Betzer, O., Shwartz, A., Motiei, M., *et al.* Nanoparticle-based CT imaging technique for longitudinal and quantitative stem cell tracking within the brain: application in neuropsychiatric disorders. ACS Nano **8,** 9274, 2014.
223. Kim, T., Lee, N., Arifin, D.R., *et al.* In vivo micro-CT imaging of human mesenchymal stem cells labeled with gold-poly-L-lysine nanocomplexes. Adv Funct Mater **27,** 1604213, 2017.
224. Zhang, Y., Thorn, S., DaSilva, J.N., *et al.* Collagen-based matrices improve the delivery of transplanted circulating progenitor cells: development and demonstration by ex vivo radionuclide cell labeling and *in vivo* tracking with positron-emission tomography. Circulation: Cardiovasc Imaging **1,** 197, 2008.
225. Chin, B., Nakamoto, Y., Bulte, J.W., Pittenger, M., Wahl, R., and Kraitchman, D. 111In oxine labelled mesenchymal stem cell SPECT after intravenous administration in myocardial infarction. Nucl Med Commun **24,** 1149, 2003.
226. Kircher, M.F., Grimm, J., Swirski, F.K., *et al.* Noninvasive in vivo imaging of monocyte trafficking to atherosclerotic lesions. Circulation **117,** 388, 2008.
227. Dorbala, S., Di Carli, M.F., Beanlands, R.S., *et al.* Prognostic value of stress myocardial perfusion positron emission tomography: results from a multicenter observational registry. J Am Coll Cardiol **61,** 176, 2013.
228. Kobylecka, M., Mączewska, J., Fronczewska-Wieniawska, K., Mazurek, T., Płazińska, M.T., and Królicki, L. Myocardial viability assessment in 18FDG PET/CT study (18FDG PET myocardial viability assessment). Nucl Med Rev **15,** 52, 2012.
229. Almutairi, A., Rossin, R., Shokeen, M., *et al.* Biodegradable dendritic positron-emitting nanoprobes for the noninvasive imaging of angiogenesis. Proc Natl Acad Sci U S A **106,** 685, 2009.
230. Sun, J., Zhou, Q., and Yang, S. Label-free photoacoustic imaging guided sclerotherapy for vascular malformations: a feasibility study. Opt Express **26,** 4967, 2018.
231. Munakata, H., Assmann, A., Poudel-Bochmann, B., *et al.* Aortic conduit valve model with controlled moderate aortic regurgitation in rats. Circ J **77,** 2295, 2013.
232. Sugimura, Y., Schmidt, A.K., Lichtenberg, A., Assmann, A., and Akhyari, P. A rat model for the in vivo assessment of biological and tissue-engineered valvular and vascular grafts. Tissue Eng Part C Methods **23,** 982, 2017.
233. Shung, K.K. Diagnostic Ultrasound: Imaging and Blood Flow Measurements. Boca Raton, FL: CRC Press, 2015.
234. Xuan, J.W., Bygrave, M., Jiang, H., *et al.* Functional neoangiogenesis imaging of genetically engineered mouse prostate cancer using three-dimensional power Doppler ultrasound. Cancer Res **67,** 2830, 2007.
235. Jugold, M., Palmowski, M., Huppert, J., *et al.* Volumetric high-frequency Doppler ultrasound enables the assessment of early antiangiogenic therapy effects on tumor xenografts in nude mice. Eur Radiol **18,** 753, 2008.
236. Christensen-Jeffries, K., Browning, R.J., Tang, M.-X., Dunsby, C., and Eckersley, R.J. In vivo acoustic super-resolution and super-resolved velocity mapping using microbubbles. IEEE Trans Med Imaging **34,** 433, 2015.
237. Kreitz, S., Dohmen, G., Hasken, S., Schmitz-Rode, T., Mela, P., and Jockenhoevel, S. Nondestructive method to evaluate the collagen content of fibrin-based tissue engineered structures via ultrasound. Tissue Eng Part C Methods **17,** 1021, 2011.
238. Rice, M.A., Waters, K.R., and Anseth, K.S. Ultrasound monitoring of cartilaginous matrix evolution in degradable PEG hydrogels. Acta Biomater **5,** 152, 2009.

239. Mercado, K.P., Helguera, M., Hocking, D.C., and Dalecki, D. Estimating cell concentration in three-dimensional engineered tissues using high frequency quantitative ultrasound. Ann Biomed Eng **42,** 1292, 2014.
240. Gudur, M.S.R., Rao, R.R., Peterson, A.W., Caldwell, D.J., Stegemann, J.P., and Deng, C.X. Noninvasive quantification of in vitro osteoblastic differentiation in 3D engineered tissue constructs using spectral ultrasound imaging. PLoS One **9,** e85749, 2014.
241. Sun, Y., Responte, D., Xie, H., *et al.* Nondestructive evaluation of tissue engineered articular cartilage using time-resolved fluorescence spectroscopy and ultrasound backscatter microscopy. Tissue Eng Part C Methods **18,** 215, 2012.
242. Garra, B.S. Imaging and estimation of tissue elasticity by ultrasound. Ultrasound Q **23,** 255, 2007.
243. Winterroth, F., Hollman, K.W., Kuo, S., *et al.* Characterizing morphology and nonlinear elastic properties of normal and thermally stressed engineered oral mucosal tissues using scanning acoustic microscopy. Tissue Eng Part C Methods **19,** 345, 2012.
244. Gudur, M., Rao, R.R., Hsiao, Y.-S., Peterson, A.W., Deng, C.X., and Stegemann, J.P. Noninvasive, quantitative, spatiotemporal characterization of mineralization in three-dimensional collagen hydrogels using high-resolution spectral ultrasound imaging. Tissue Eng Part C Methods **18,** 935, 2012.
245. Kim, K., Jeong, C.G., and Hollister, S.J. Non-invasive monitoring of tissue scaffold degradation using ultrasound elasticity imaging. Acta Biomater **4,** 783, 2008.
246. Yu, J., Takanari, K., Hong, Y., *et al.* Non-invasive characterization of polyurethane-based tissue constructs in a rat abdominal repair model using high frequency ultrasound elasticity imaging. Biomaterials **34,** 2701, 2013.
247. Teodori, L., Crupi, A., Costa, A., Diaspro, A., Melzer, S., and Tarnok, A. Three-dimensional imaging technologies: a priority for the advancement of tissue engineering and a challenge for the imaging community. J Biophotonics **10,** 24, 2017.
248. Dittmar, R., Potier, E., van Zandvoort, M., and Ito, K. Assessment of cell viability in three-dimensional scaffolds using cellular auto-fluorescence. Tissue Eng Part C Methods **18,** 198, 2011.
249. Fu, D., Matthews, T.E., Ye, T., Piletic, I., and Warren, W.S. Label-free in vivo optical imaging of microvasculature and oxygenation level. J Biomed Opt **13,** 040503, 2008.
250. So, P.T., Dong, C.Y., Masters, B.R., and Berland, K.M. Two-photon excitation fluorescence microscopy. Ann Rev Biomed Eng **2,** 399, 2000.
251. Georgakoudi, I., Rice, W.L., Hronik-Tupaj, M., and Kaplan, D.L. Optical spectroscopy and imaging for the noninvasive evaluation of engineered tissues. Tissue Eng Part B Rev **14,** 321, 2008.
252. Rice, W.L., Firdous, S., Gupta, S., *et al.* Non-invasive characterization of structure and morphology of silk fibroin biomaterials using non-linear microscopy. Biomaterials **29,** 2015, 2008.
253. Sun, Y., Tan, H.Y., Lin, S.J., *et al.* Imaging tissue engineering scaffolds using multiphoton microscopy. Microsc Res Tech **71,** 140, 2008.
254. Zhang, Y.S., Wang, Y., Wang, L., *et al.* Labeling human mesenchymal stem cells with gold nanocages for in vitro and in vivo tracking by two-photon microscopy and photoacoustic microscopy. Theranostics **3,** 532, 2013.
255. Shih, A.Y., Driscoll, J.D., Drew, P.J., Nishimura, N., Schaffer, C.B., and Kleinfeld, D. Two-photon microscopy as a tool to study blood flow and neurovascular coupling in the rodent brain. J Cereb Blood Flow Metab **32,** 1277, 2012.
256. Tan, W., Oldenburg, A.L., Norman, J.J., Desai, T.A., and Boppart, S.A. Optical coherence tomography of cell dynamics in three-dimensional tissue models. Opt Express **14,** 7159, 2006.
257. Yang, Y., Dubois, A., Qin, X.-P., Li, J., El Haj, A., and Wang, R.K. Investigation of optical coherence tomography as an imaging modality in tissue engineering. Phys Med Biol **51,** 1649, 2006.
258. Liang, X., Graf, B.W., and Boppart, S.A. Imaging engineered tissues using structural and functional optical coherence tomography. J Biophotonics **2,** 643, 2009.
259. Wei, W., Choi, W.J., and Wang, R.K. Microvascular imaging and monitoring of human oral cavity lesions in vivo by swept-source OCT-based angiography. Lasers Med Sci **33,** 123, 2018.
260. Davoudi, B., Lindenmaier, A., Standish, B.A., Allo, G., Bizheva, K., and Vitkin, A. Noninvasive in vivo structural and vascular imaging of human oral tissues with spectral domain optical coherence tomography. Biomed Opt Express **3,** 826, 2012.
261. Davoudi, B., Morrison, M., Bizheva, K., *et al.* Optical coherence tomography platform for microvascular imaging and quantification: initial experience in late oral radiation toxicity patients. J Biomed Opt **18,** 076008, 2013.
262. Choi, W.J., Pepple, K.L., Zhi, Z., and Wang, R.K. Optical coherence tomography based microangiography for quantitative monitoring of structural and vascular changes in a rat model of acute uveitis in vivo: a preliminary study. J Biomed Opt **20,** 016015, 2015.
263. Leitgeb, R.A., Werkmeister, R.M., Blatter, C., and Schmetterer, L. Doppler optical coherence tomography. Prog Retin Eye Res **41,** 26, 2014.
264. Chen, C.-W., Betz, M.W., Fisher, J.P., Paek, A., and Chen, Y. Macroporous hydrogel scaffolds and their characterization by optical coherence tomography. Tissue Eng Part C Methods **17,** 101, 2010.
265. Levitz, D., Hinds, M.T., Choudhury, N., Tran, N.T., Hanson, S.R., and Jacques, S.L. Quantitative characterization of developing collagen gels using optical coherence tomography. J Biomed Opt **15,** 026019, 2010.
266. Veksler, B.A., Kuz'min, V.L., Kobzev, E., and Meglinski, I.V. The use of optical coherence tomography for morphological study of scaffolds. Quantum Electron **42,** 394, 2012.
267. White, B.R., Pierce, M.C., Nassif, N., *et al.* In vivo dynamic human retinal blood flow imaging using ultra-high-speed spectral domain optical Doppler tomography. Optics express **11,** 3490, 2003.
268. Wang, Y., Bower, B.A., Izatt, J.A., Tan, O., and Huang, D. In vivo total retinal blood flow measurement by Fourier domain Doppler optical coherence tomography. J Biomed Opt **12,** 041215, 2007.
269. Wang, X., Xie, X., Ku, G., Wang, L.V., and Stoica, G. Noninvasive imaging of hemoglobin concentration and oxygenation in the rat brain using high-resolution photoacoustic tomography. J Biomed Opt **11,** 024015, 2006.

270. Zhang, H.F., Maslov, K., Sivaramakrishnan, M., Stoica, G., and Wang, L.V. Imaging of hemoglobin oxygen saturation variations in single vessels in vivo using photoacoustic microscopy. Appl Phys Lett **90,** 053901, 2007.
271. Ning, B., Kennedy, M.J., Dixon, A.J., *et al.* Simultaneous photoacoustic microscopy of microvascular anatomy, oxygen saturation, and blood flow. Optics Lett **40,** 910, 2015.
272. Buehler, A., Herzog, E., Razansky, D., and Ntziachristos, V. Video rate optoacoustic tomography of mouse kidney perfusion. Opt Lett **35,** 2475, 2010.
273. Siphanto, R., Thumma, K., Kolkman, R., *et al.* Serial noninvasive photoacoustic imaging of neovascularization in tumor angiogenesis. Opt Express **13,** 89, 2005.
274. Yao, J., Maslov, K.I., Shi, Y., Taber, L.A., and Wang, L.V. *In vivo* photoacoustic imaging of transverse blood flow by using Doppler broadening of bandwidth. Opt Lett **35,** 1419, 2010.
275. Zhang, Y.S., Cai, X., Yao, J., Xing, W., Wang, L.V., and Xia, Y. Non-invasive and in situ characterization of the degradation of biomaterial scaffolds by volumetric photoacoustic microscopy. Angew Chem Int Ed **53,** 184, 2014.
276. Zhang, Y.S., Wang, L.V., and Xia, Y. Seeing through the surface: non-invasive characterization of biomaterial–tissue interactions using photoacoustic microscopy. Ann Biomed Eng **44,** 649, 2016.

Address correspondence to:
Eric M. Brey, PhD
Department of Biomedical Engineering
University of Texas at San Antonio
One UTSA Circle
San Antonio, TX 78249-0712

E-mail: eric.brey@utsa.edu

Received: October 31, 2019
Accepted: December 13, 2019
Online Publication Date: January 14, 2020